ARTICLE OPEN ACCESS

Experimental and Comparative Study of the Corrosion Behavior of Lean Duplex Stainless Steel in Seawater

Mohammad Hassanzadeh[1,2] | Nicolas Larché[1] | Audrey Allion-Maurer[3] | Raf Dewil[2,4] | Barbara Rossi[2,4]

[1]Institut de la Corrosion (French Corrosion Institute), Brest, France | [2]Department of Chemical Engineering, KU Leuven, Leuven, Belgium | [3]Isbergues Research Center, APERAM Stainless Steel, Isbergues, France | [4]Department of Engineering Science, University of Oxford, Oxford, UK

Correspondence: Nicolas Larché (nicolas.larche@institut-corrosion.fr)

Received: 18 February 2026 | **Revised:** 25 March 2026 | **Accepted:** 18 April 2026

Funding: Horizon Europe Marie Skłodowska-Curie Actions, Grant/Award Number: 101073471

Keywords: austenitic stainless steel | crevice corrosion | duplex stainless steel | pitting corrosion | seawater

ABSTRACT

This study investigates the localized corrosion resistance of lean duplex stainless steel S32202 (EN 1.4062) in natural seawater. Its performance is compared to that of austenitic stainless steel 316 L (EN 1.4404), standard duplex S32205 (EN 1.4462), and super duplex S32750 (EN 1.4410) stainless steels. Crevice and pitting corrosion tests are conducted following the ISO 18070:2015 and ASTM G150 standards, respectively. The results indicate that EN 1.4062 exhibits superior critical pitting temperature and higher crevice corrosion resistance compared with EN 1.4404. Under a severe combination of conditions: a 20°C water temperature, a gasket pressure of 20 N/mm^2, and a surface roughness of $Ra = 0.3 \pm 0.1$ µm, even the higher-grade EN 1.4462 and EN 1.4410 may be susceptible to crevice corrosion. These findings suggest that EN 1.4062 may be suitable for certain short-term seawater applications, either independently or in combination with corrosion protection strategies.

1 | Introduction

Various offshore industries, including fossil fuel and renewable energy, fishing and aquaculture, are subjected to severely corrosive environments. The reliability and sustainability of their infrastructure are crucial to their profitability and largely depend on the use of strong and corrosion-resistant metal alloys (CRAs) [1–4]. Stainless steel (SS), a type of CRA, has a wide range of applications in seawater environments [5–8]. They are classified into four families based on their crystalline microstructure: ferritic, austenitic, martensitic, and duplex [9]. Despite their ability to form a self-repairing corrosion-resistant oxide layer, stainless steels remain susceptible to localized forms of corrosion, particularly pitting and crevice corrosion in harsh environments [2, 5, 10–12].

The relative resistance of different grades to localized corrosion is typically assessed using the pitting resistance equivalent number (PREN), as defined by the following equation [6, 7, 13–15]:

$$PREN = \%Cr + 3.3\%Mo + 16\,\%N \quad (1)$$

It is widely accepted that stainless steels with a PREN greater than 40 offer reliable long-term corrosion resistance in seawater [6, 7, 10]. Accordingly, the so-called 6Mo austenitic alloy, with approximately 6% Mo and $PREN \geq 40$, and 25Cr duplex alloy with a PREN between 40 and 45 [16] have been frequently recommended for seawater applications up to 20°C, including those immersed [6, 7]. However, the selection of materials for use in natural seawater environments must take into account multiple criteria to ensure optimal performance, durability, alongside cost-effectiveness, depending on tensile strength, material cost, availability, ease of fabrication, and corrosion resistance in the specific operational conditions of the application.

Duplex stainless steels (DSSs), characterized by their dual-phase ferrite/austenite microstructure, provide corrosion resistance comparable to that of austenitic stainless steels while offering superior tensile strength [8, 13, 17–22]. The higher strength of DSSs compared to austenitic stainless steels typically allows for reduced material thickness, thereby lowering overall material cost. Additionally, DSSs generally contain less Ni, significantly reducing costs and cost volatility compared to highly (Ni)alloyed CRAs [19, 23, 24] offering notable cost advantages over austenitic stainless steels.

The modern DSS family is categorized into four primary groups: lean, standard, super, and hyper DSS [14]. Their Ni and Mo contents, which largely dictate material costs, decrease progressively from hyper DSS to lean DSS [15, 25]. Although a reduced alloying content results in a lower PREN and thus presumably also a decreased localized corrosion resistance (lean DSS compared to more highly alloyed DSS grades), this reduction is accompanied by significantly enhanced cost-effectiveness. Consequently, in scenarios involving short-term seawater immersion (e.g., internal surfaces of subsea pipelines between installation and operational start-up) or in cases where protective measures (such as cathodic protection) mitigate corrosion, lean DSS offer a cost-effective and adequately resistant material choice.

2 | State-of-the-Art

Based on the results of a Scopus search, among 129 journal and conference publications since 2010 addressing the corrosion of duplex and superaustenitic stainless steels in seawater, lean DSS grades have received the least attention, with only nine papers (7%) focusing on them. Among the nine studies addressing the corrosion behavior of lean DSSs in seawater, seven focused on grade S32101 (EN 1.4162), five examined S32304 (EN 1.4362), and only one investigated S32202 (EN 1.4062). The latter study, conducted by Larché et al. [5], analyzed the localized corrosion behavior in deep seawater and compared three lean DSS grades (EN 1.4062, EN 1.4162, and EN 1.4362) with other grades, including duplex, ferritic, austenitic, super-austenitic stainless steels, and Ni-based alloys. Their findings revealed the following corrosion resistance ranking: 1.4404 < 1.4162 < 1.4062 < 1.4362 << 1.4462 << (1.4410, 1.4477, 1.4652, 1.4432). The remaining eight studies explored various factors influencing the corrosion behavior of lean DSS. Breda et al. [26] investigated the effects of cold rolling on the pitting corrosion resistance and reported a 25% and a 15% reduction in the critical pitting temperature (CPT) for S32101 (EN 1.4162) and S32304 (EN 1.4362), respectively. Gong et al. [27] reported a beneficial impact of cerium (Ce) on the corrosion resistance of S32101 (EN 1.4162). Pezzato et al. [28] assessed how secondary phase precipitation affects the corrosion resistance of DSS. Ohashi et al. [29] compared the corrosion behavior of DSS grades, including S32101 (EN 1.4162), in sterile and microbially active seawater environments at 30°C. Srisungsitthisunti et al. [30] utilized short-term electrochemical tests, such as cyclic potentiodynamic polarization and potentiostatic techniques, to evaluate crevice corrosion of S31600 (EN 1.4401), S32101 (EN 1.4162), S31803 (EN 1.4462), and S32750 (EN 1.4410) in the 3.5% NaCl solution. Ming et al. [31] used the electrochemical impedance spectroscopy (EIS) method to examine the corrosion behavior of S32304 (EN 1.4362) as a reinforcing bar in seawater-mixed concrete. Gennari et al. [32] analyzed the effect of welding heat input on the critical pitting temperature (CPT) of different welded S32304 (EN 1.4362) components produced by laser beam welding process. Chang et al. [33] investigated the suitability of lean DSSs under high-flow-velocity seawater conditions relevant to nuclear power plant applications, using potentiodynamic polarization and CPT tests [5].

Given the promising advantages of lean DSSs, precisely defining their operational limits is essential. Therefore, in this study, the localized corrosion behavior of lean DSS EN 1.4062 (S32202) is compared with that of EN 1.4404 (S31603) austenitic stainless steel as a lower reference, and with EN 1.4462 (S32205) standard DSS and EN 1.4410 (S32750) super DSS as upper references. Compared to Larché et al. [5] study, the test medium temperature for the crevice test is increased to 20°C, and the ASTM G150 [34] test method is employed to rank the material grades in terms of their pitting corrosion resistance.

3 | Experimental Procedure

3.1 | Materials

The materials used in this study were extracted from thin plates with a thickness in the range of 3–5 mm. Table 1 presents the chemical compositions of the four stainless steel grades evaluated in this study. These compositions comply with the European standard of EN 10088-1 [35]. Figure 1 shows their measured microstructures both in the rolling (Figure 1a,c,e,g) and transversal (Figure 1b,d,f,h) directions. The micrographs were obtained via a Leica DMC-2900 optical microscope following a four-step polishing procedure. Polishing began with 220-grit sandpaper, followed by the use of 9 and 3 μm particles in the second and third steps, and concluded with a final polishing stage using 0.04 μm particles. Etching was performed using 1 N NaOH at 1.8 V for grade 1.4410 and at 2.2 V for grades 1.4462 and 1.4062, whereas saturated oxalic acid at 0.4 A was used for the austenitic grade (1.4404). As depicted in Figure 1, grade 1.4404 exhibits a single-phase austenitic microstructure, whereas the three duplex (DSS) grades show a microstructure comprising both austenite and ferrite. No secondary phases, such as

TABLE 1 | Chemical compositions of 1.4404, 1.4062, 1.4462, and 1.4410.

EN no.	Grades	UNS no.	C	Ni	Cr	Mo	N	Mn	Cu	P	S	Fe
1.4404	316L	S31603	0.025	10.0	16.7	2.0	0.050	1.2	0.30	0.030	16 ppm	Bal.
1.4062	2202	S32202	0.023	2.6	23.1	0.2	0.192	1.3	0.22	0.030	5 ppm	Bal.
1.4462	2205	S32205	0.013	5.5	22.7	3.1	0.171	1.8	0.20	0.030	6 ppm	Bal.
1.4410	2507	S32750	0.017	6.7	25.5	3.7	0.250	0.8	0.30	0.032	4 ppm	Bal.

Note: All chemical compositions have been reported in weight percentage except for S.
Abbreviation: Bal., balanced.

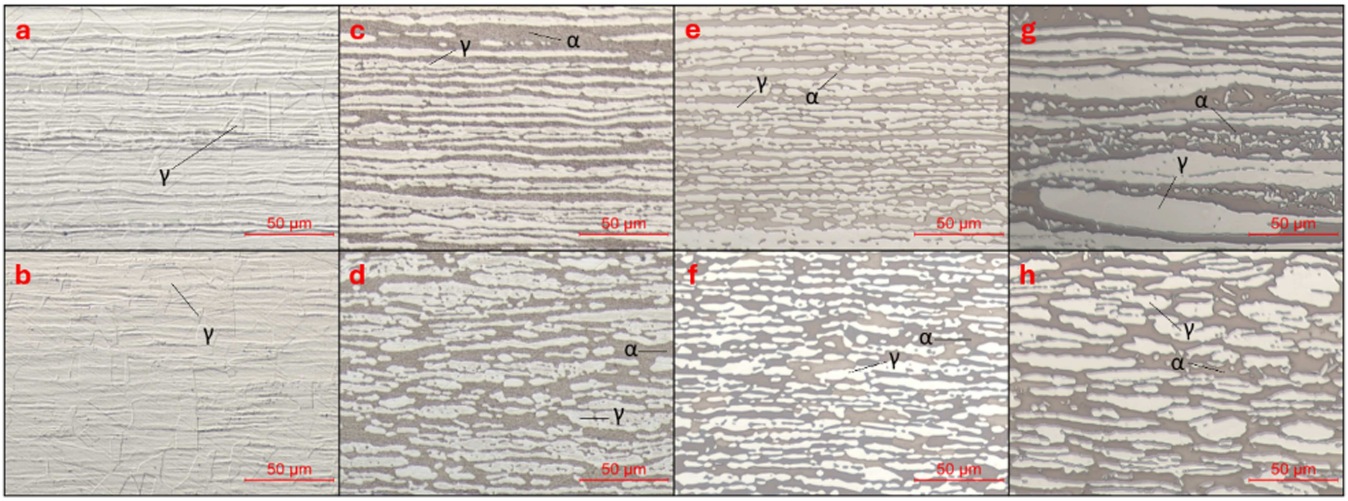

FIGURE 1 | (a, b) Microstructures of 1.4404 in the rolling and transversal directions, respectively; (c, d) corresponds to 1.4062; (e, f) to 1.4462; and (g, h) to 1.4410. The ferrite (α) phase appears dark, while the austenite (γ) phase appears light. [Color figure can be viewed at wileyonlinelibrary.com]

TABLE 2 | Ferrite and austenite fractions for the three tested DSS grades, obtained via quantitative image analysis.

Fraction	Field1		Field2		Field3		Field4		Average		
Grade	%α	%γ	%α	%γ	%α	%γ	%α	%γ	%α	%γ	Std
1.4062 (2202)	45.0	55.0	53.5	46.5	47.3	52.7	51.6	48.4	49.4	50.6	3.4
1.4462 (2205)	50.2	49.8	50.6	49.4	59.2	40.8	57.3	42.7	54.3	45.7	4.0
1.4410 (2507)	58.6	41.4	53.6	46.4	54.1	45.9	52.2	47.8	54.6	45.4	2.4

intermetallic phases (σ, χ, α') or carbides and nitrides, were observed, ensuring material integrity [15, 36, 37].

As shown in Table 2, the ferrite-austenite phase fractions were determined for three DSS samples using quantitative image analysis in accordance with ASTM E1245 [38]. Image segmentation was performed using Otsu's automatic thresholding method implemented in ImageJ, and the results were validated using point counting in accordance with ASTM E562 [39]. This measurement was done on four fields (two in the rolling direction and two in the transversal direction) with 50× magnification for each grade. The measured phase fractions for all three DSS grades are within the acceptable range of 35%–60% [37, 40].

3.2 | Specimen Preparation for Pitting and Crevice Corrosion Tests

For the CPT tests, three specimens measuring 45 × 45 mm with thicknesses ranging 3–5 mm were cut from each of the four studied grades. These specimens were polished sequentially in seven stages via sandpaper with grit sizes of 80, 120, 220, 320, 500, 800, and 1200. The specimens were subsequently cleaned in an ultrasonic bath containing a 50% acetone-50% ethanol solution for 5 min and then dried with air blowing. Prior to testing, the specimens were stored at room temperature for at least 16 h to allow for atmospheric repassivation [34].

In addition to pitting, crevice corrosion poses significant threat to stainless steels in seawater, and it is often more prevalent than pitting [2, 11, 12]. Crevice conditions can arise between two contacting structural components, within gaps smaller than 500 µm, or beneath microorganisms attached to the metal surface [2].

For the crevice test, specimens were fabricated from plates measuring 150 × 100 mm. The number and thickness of the specimens for each material grade are presented in Table 3. A total of 15 specimens were prepared for each material grade except for the super DSS (1.4410). Since the super DSS has a PREN value greater than 40 [6, 7], no corrosion was anticipated during short-term immersion, which is also in agreement with industrial standards [6, 7]. Thus, only five super DSS samples were prepared for extraction from the testing medium after 6 months. To prevent pitting corrosion [41] via an angle grinder equipped with a flap disc [42].

For the crevice test specimens, two holes with diameters of 4.5 and 9 mm were drilled at the top and center, respectively, to accommodate the titanium Grade 2 connector and crevice former assembly. As illustrated in Figure 2 and in accordance with ISO 18070:2015 [41], the crevice condition was established via an assembly consisting of two polyvinylidene fluoride (PVDF) gaskets, two washers, one nut, and an insulated titanium Grade 2 bolt. To intensify the crevice conditions, standard ISO 18070:2015 parameters were adjusted by increasing the gasket pressure to approximately 20 N/mm^2 (applied by a torque wrench set at 20 N·m) and reducing the surface roughness of the circular crevice region to Ra = 0.3 ± 0.1 µm [5, 21, 43, 44] through a three-step polishing process (sandpaper grit sizes: 80, 180, 600). These modifications aimed to better simulate industrial applications, such as threaded connections, flanges, and sealing components [45]. The surface

TABLE 3 | Number of samples per material grade used for the crevice test, and the corresponding thicknesses.

Material grade	Thickness (mm)	No. of specimens
1.4404	3	15
1.4062	4	15
1.4462	3	15
1.4410	5	5

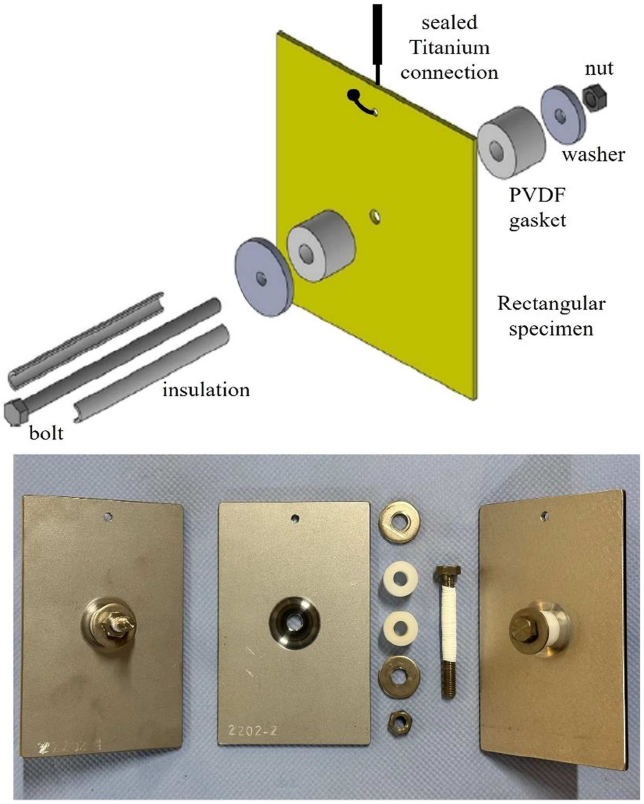

FIGURE 2 | Crevice test assembly, consisting of a test plate, electrical connection, and crevice former elements. [Color figure can be viewed at wileyonlinelibrary.com]

roughness of the crevice region was verified using vertical scanning interferometry (VSI) to ensure reproducibility. The area ratio between the crevice region and the remaining specimen surface was approximately 1:60. Additionally, the PVDF gasket surfaces were polished with grit-600 (P1200) sandpaper to achieve uniform surface conditions across all the crevice formers. Moreover, 24 h before initiating the crevice test, the samples were ultrasonically cleaned in ethanol for 10 min and then passivated in a 25 vol% nitric acid solution at room temperature for 30 min [46]. Prior to tightening the crevice former using a torque wrench, the plates were pre-wetted by soaking in water, a step intended to minimize variations in seawater diffusion within the crevice region.

3.3 | Pitting Corrosion Test Setup and Procedure

To compare the pitting resistance of the four grades, their critical pitting temperature (CPT) was measured according to the ASTM G150 standard [34]. CPT is defined as the lowest temperature at which stable and propagating pitting corrosion occurs, independent of the applied potential. This accelerated corrosion test serves primarily as a ranking method for material performance rather than simulating actual service conditions. A flushed-port cell (AVESTA cell), as illustrated in Figure 3, was used for conducting the CPT measurements. The cell was filled with 1 L of a 1 M NaCl solution and continuously purged with high-purity nitrogen gas (99.99%) throughout the test. Nitrogen purging was employed solely to ensure adequate stirring and not for oxygen removal, as the oxygen concentration does not affect the test outcome [34]. The test area of each specimen was circular, with an area of 4.9 cm^2.

After lowering the solution temperature below 3°C, the test began with open circuit potential (OCP) monitoring for 1 h, the temperature was subsequently increased at a rate of 1°C per min. A thermocouple with a measurement accuracy of ±0.4°C monitored the temperature, whereas a temperature controller coupled with a thermostat regulated the cooling and heating rates. In addition, 60 s prior to initiating the temperature increase, the specimen was anodically polarized to a potential exceeding its pitting potential range. The CPT test is potentiostatic, meaning that the potential is maintained at a constant value above the material's pitting potential at 25°C; for stainless steel, this value is typically +700 mV versus SCE. A GAMRY Interface 1010E potentiostat was used for conducting the test.

During the test, the current density was continuously monitored. When the current density exceeded 100 $\mu A/cm^2$ and remained above this threshold for at least 60 s (to ensure that the increase was not due to a metastable pitting), the corresponding temperature was recorded as the CPT.

Upon reaching the CPT, the specimens were removed from the test cell, rinsed with distilled water followed by 95% ethanol, and dried with compressed air. The specimen surfaces were then examined visually and under binocular and 3D microscopes to confirm pitting. The observation of pits was essential to validate the CPT results; if no pitting was detected, the test was repeated [34].

3.4 | Crevice Corrosion Test Setup and Procedure

The crevice test was performed in a non-metallic exposure tank containing approximately 300 L of natural seawater. To closely replicate marine immersion conditions, seawater from Brest Bay, France, was continuously pumped into the tank from depths between 5 and 10 m below the sea surface. The seawater was renewed at a flow rate of 300 L/day, ensuring complete replacement of the tank volume every 24 h. As depicted in Figure 4, the natural seawater temperature during the test period fluctuated between 12°C and 18°C. However, as temperature is known to increase the corrosiveness of seawater, the test medium temperature was maintained constant at an ambient temperature level of 20 ± 3°C via a temperature-controlled heater. Additionally, a pump circulated seawater within the tank to ensure homogeneous conditions.

Other environmental parameters, including dissolved oxygen (DO), pH, and salinity, were maintained at levels comparable to those of in situ seawater conditions in Brest Bay, France. As

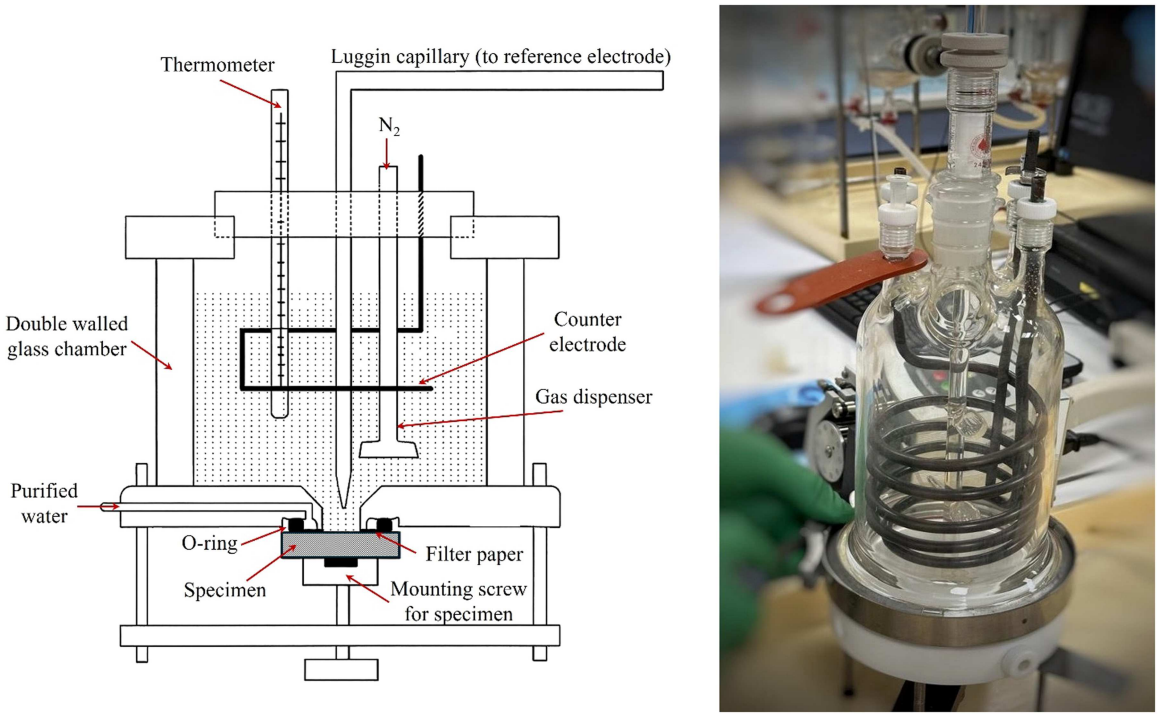

FIGURE 3 | Left: sketch of the CPT test cell adapted from the ASTM G150 standard [34], and right: the actual used AVESTA cell. [Color figure can be viewed at wileyonlinelibrary.com]

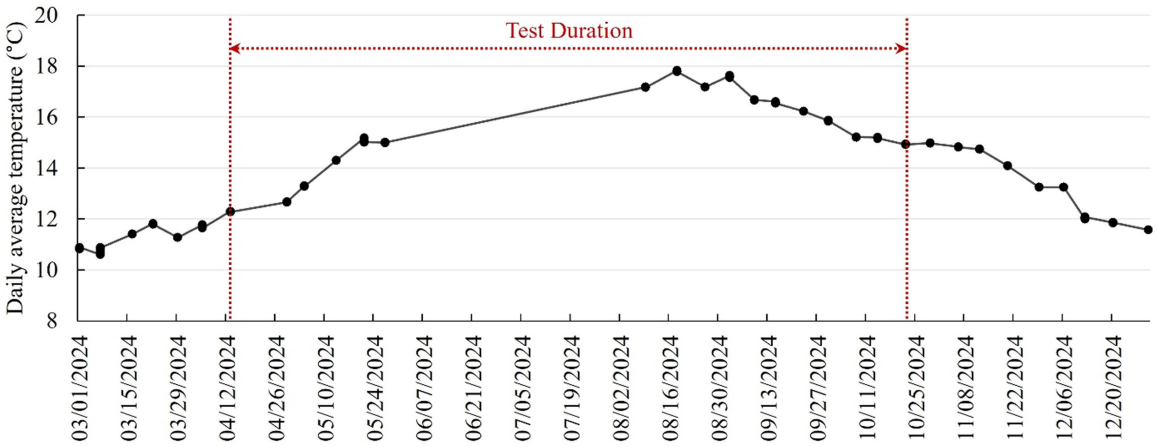

FIGURE 4 | Temperature trend of intake seawater taken from Brest Bay, France (before regulation at 20 ± 3°C in the exposure tank) [47]. [Color figure can be viewed at wileyonlinelibrary.com]

illustrated in Figure 5, the pH remained within a narrow range of 7.8–8.0, whereas the dissolved oxygen content exhibited a relatively stable pattern, fluctuating between 5 and 7 mL/L. Salinity increased from 33.5 to 35 PSU due to seasonal variations.

During the immersion period (6 months), the open circuit potential (OCP) of the specimens was continuously logged at a frequency of one reading every 30 min. The potentials were measured against an Ag-AgCl/KCl-gel electrode calibrated with a saturated calomel electrode (SCE). A high-impedance data logger ($> 10^{11}$ Ω), suitable for electrochemical measurements, was used to record the potential.

Five specimens were removed from the tank at three distinct intervals, corresponding to approximately 1, 3, and 6 months of immersion, representing short-, mid-, and long-term exposure, respectively. Due to operational constraints, the actual removal times were 35, 90, and 184 days, during which continuous OCP monitoring was conducted. For 1.4410 grade, specimens were collected only after 184 days. At each removal interval, priority was given to the selection of corroded specimens. After removal, the specimens were rinsed with tap water and then placed in an ultrasonic bath containing a 25 vol% nitric acid solution to remove all the corrosion products.

The depth, area, and profile of the specimens' corroded zones were measured and analyzed in relation to the OCP trend. These analyses were conducted using the focalization method combined with OM, VSI microscope, and JMicroVision image-analysis software, as shown in Figure 6. In addition, the microstructure of the corroded surfaces was examined via OM, and a Hitachi SU 3500 scanning electron microscope (SEM) associated with energy dispersive spectroscopy (EDS) was used to assess the corrosion mechanism.

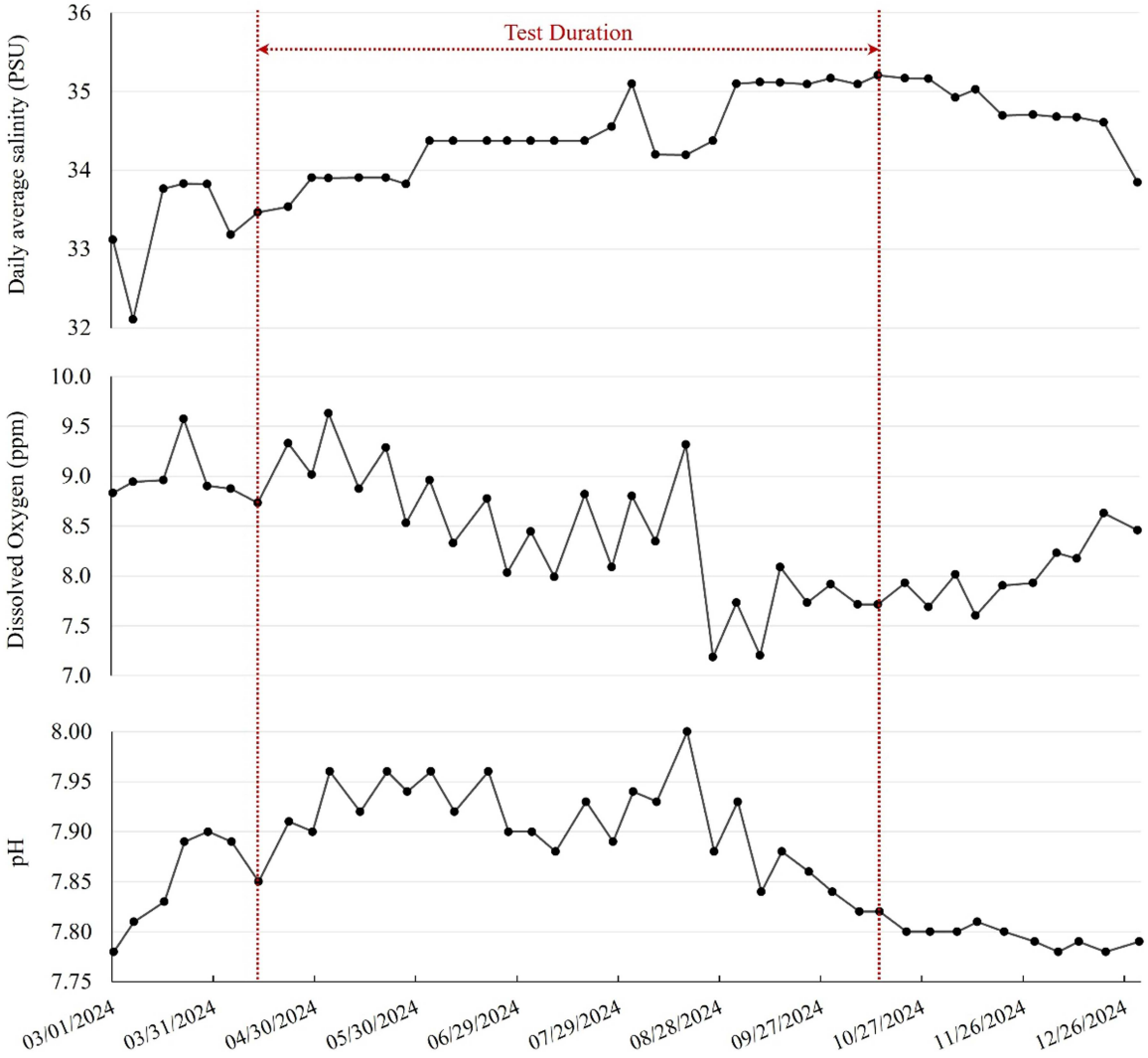

FIGURE 5 | Environmental parameters during the test duration, including salinity, dissolved oxygen, and pH [47]. [Color figure can be viewed at wileyonlinelibrary.com]

4 | Results

4.1 | Pitting Test Results

Figure 7 illustrates the variation in current density as a function of temperature. The critical pitting temperatures (CPTs) are the points at which the current density exceeds 100 $\mu A/cm^2$ (depicted with red bullets on the graphs) and remains above this threshold for at least 60 s (the time interval corresponding to a temperature increment of 1°C) [34].

Table 4 presents the CPTs for the four grades. Considering the standard deviations, the results demonstrate very good reproducibility. The CPTs of the four grades are clearly distinguishable, with significantly different values of 13.1, 29.9, 56.0, and 89.5°C for grades 1.4404, 1.4062, 1.4462, and 1.4410, respectively. The distinguishability is further emphasized by calculating the ratios between the CPT of each grade and the CPT of 1.4404 austenitic stainless steel as the baseline reference. These ratios reveal an approximately twofold increase between each successive material in the series. Notably, for grade 1.4410, two replicates reached the maximum operational temperature of the experimental setup (90°C) with the current density well below the 100 $\mu A/cm^2$ threshold, indicating a very low susceptibility to pitting corrosion for this grade.

Due to its specific test conditions, the CPT method is primarily used to rank material grades rather than to represent their actual corrosion behavior in service environments. Table 5 presents the PREN (Equation 1) of the four tested grades, calculated with their chemical compositions from Table 1.

A comparison of Tables 4 and 5 reveals that, while the PREN values in Table 5 suggest very close pitting resistance for grades 1.4404 and 1.4062, the CPT results in Table 4 clearly indicate distinct pitting resistance ranges. This discrepancy likely arises from the fact that PREN is calculated solely based on the chemical composition of specific alloying elements. As a result, several influential factors, such as other alloying elements, metallurgical quality, and surface finish, are not accounted for in the PREN calculation, potentially leading to an unadopted assessment of actual corrosion resistance [48].

Figure 8 shows that the PREN exhibits a quasi-linear relationship with the CPT values for the three commonly used grades 1.4404, 1.4462, and 1.4410, which is consistent with the trend reported in

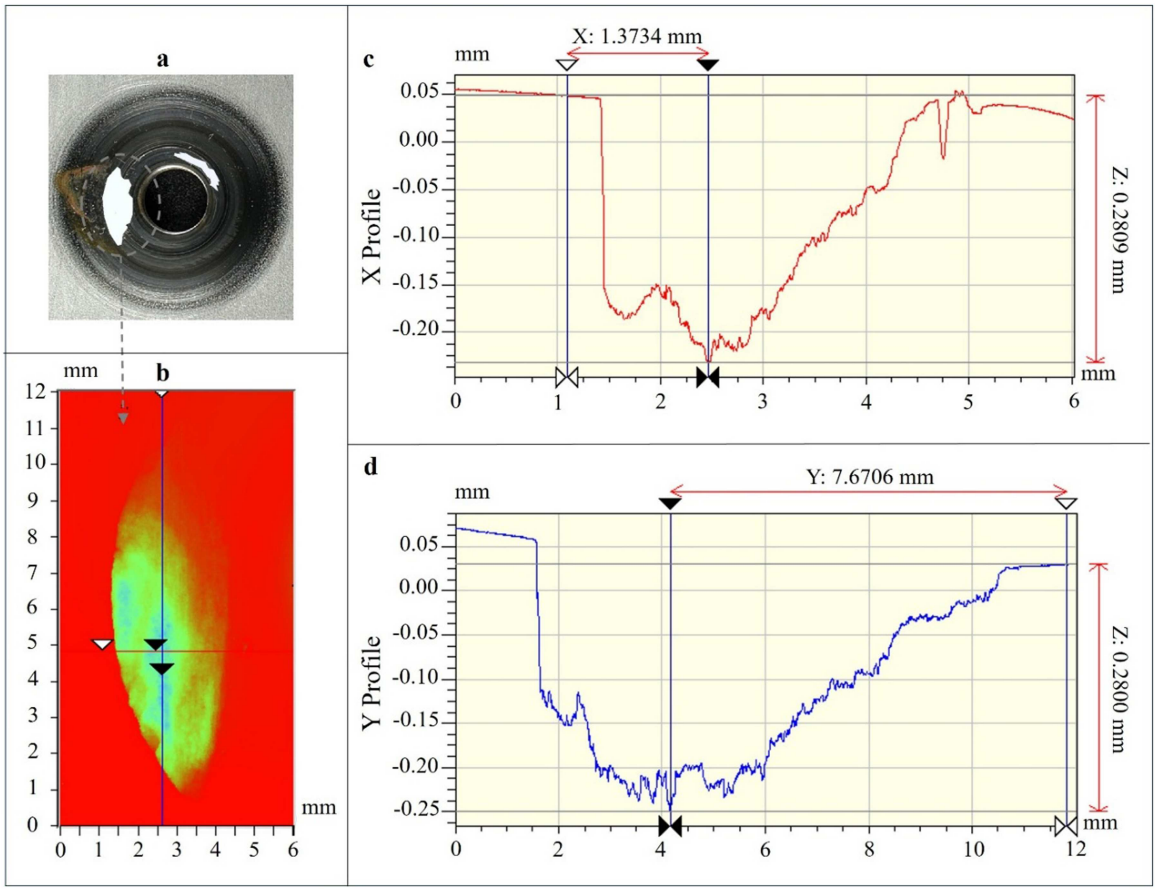

FIGURE 6 | Corrosion profile of a typical 1.4462 specimen. (a) Macro-photo of the crevice region, (b) corroded area picture by VSI, (c) corrosion depth profile along the *X*-axis, and (d) corrosion depth profile along the *Y*-axis. [Color figure can be viewed at wileyonlinelibrary.com]

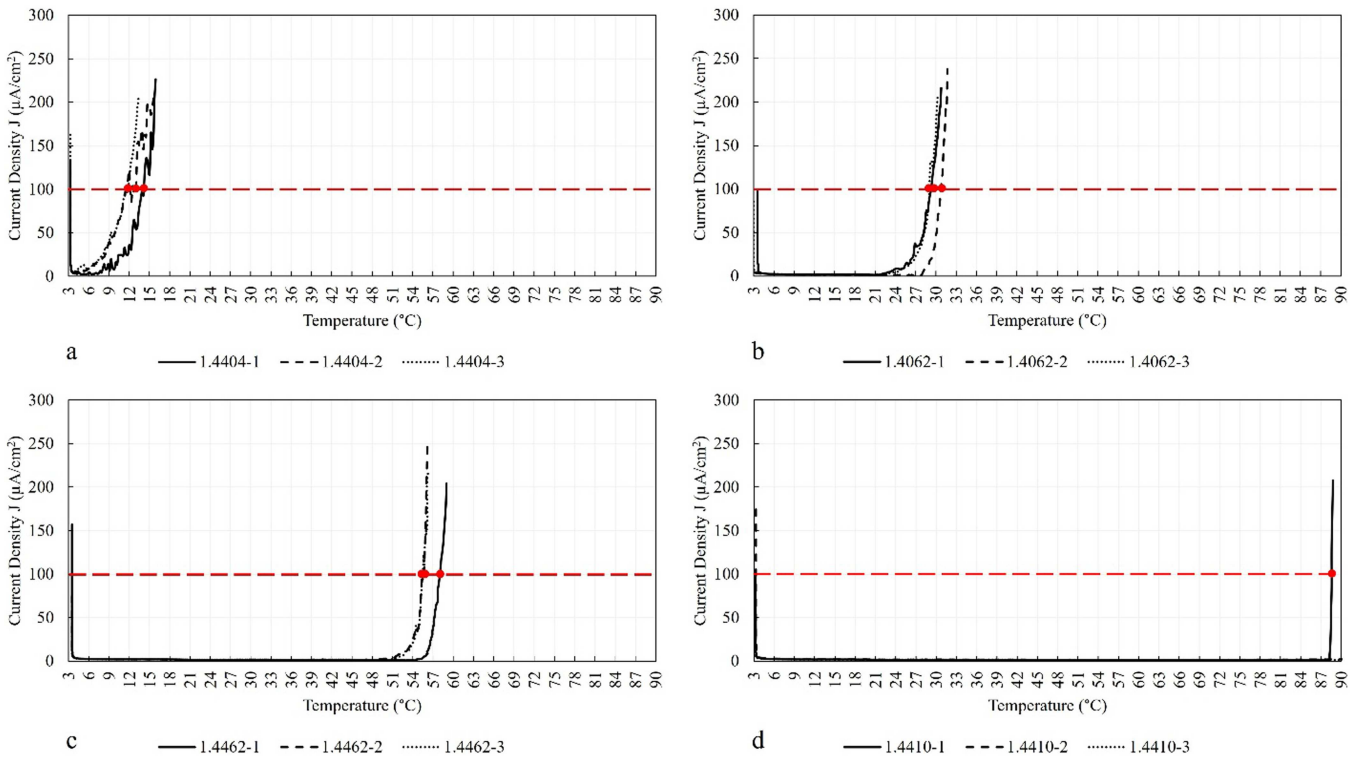

FIGURE 7 | Current density records versus temperature for (a) 1.4404, (b) 1.4062, (c) 1.4462, and (d) 1.4410. [Color figure can be viewed at wileyonlinelibrary.com]

TABLE 4 | CPT test results for the four grades.

Grades	CPT (°C)			STD EV.P	Average CPT	CPT changing ratio
	1	2	3			
1.4404	14.3	13.2	11.8	1.0	13.1	1.0
1.4062	29.5	30.9	29.2	0.7	29.9	2.3
1.4462	57.3	55.1	55.6	0.9	56.0	4.3
1.4410	88.6	> 90[a]	> 90[a]	0.7	89.5	6.8

[a]The maximum operation temperature of the test setup is 90°C.

TABLE 5 | PREN of the four grades calculated by applying the actual chemical compositions (in weight percent) from Table 1 into Equation (1).

Grades	PREN	Change ratio
1.4404	24.1	1.0
1.4062	26.8	1.1
1.4462	35.7	1.5
1.4410	41.7	1.7

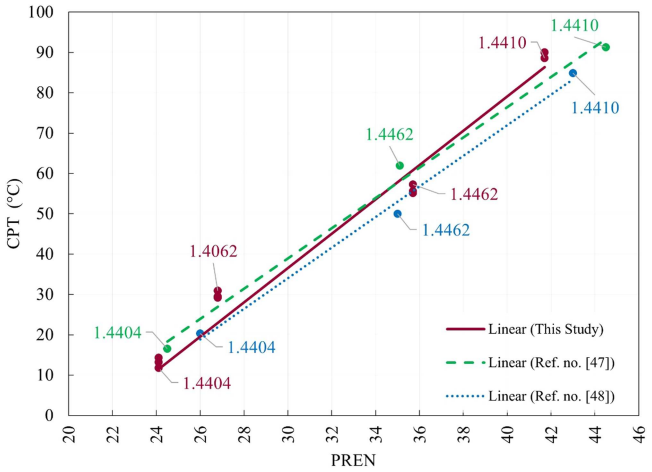

FIGURE 8 | CPT versus PREN changes for four grades. Red: linear regression and data obtained via this study. Green: linear regression and data adapted from [49]; blue: linear regression and data adapted from [50]. [Color figure can be viewed at wileyonlinelibrary.com]

the literature [15, 49, 50]. However, grade 1.4062 locates above the fitted lines from this study and literature suggesting that despite the limitted difference in PREN values, 26.8 versus 24.1 for 1.4062 and 1.4404, respectively, the 1.4062 lean DSS can be significantly more resistant to pitting corrosion than the 1.4404 austenitic stainless steel considering CPT of 29.9°C versus 13.1°C for 1.4062 and 1.4404, respectively.

Microscopic inspections confirmed the CPT test results, revealing denser and deeper pitting in the lower-resistance grades. By microscopic evaluation, numerous pits were observed on the surface of grade 1.4404, while for duplex grades, individual pits were observed. The maximum corrosion depth on the 1.4404, 1.4062 (shown as an example in Figure 9), and 1.4462 specimens was 72, 42, and 8 μm (shallow etching < 25 μm), respectively. The grade 1.4410 exhibited only a superficial attack with a depth of less than 5 μm [5, 48].

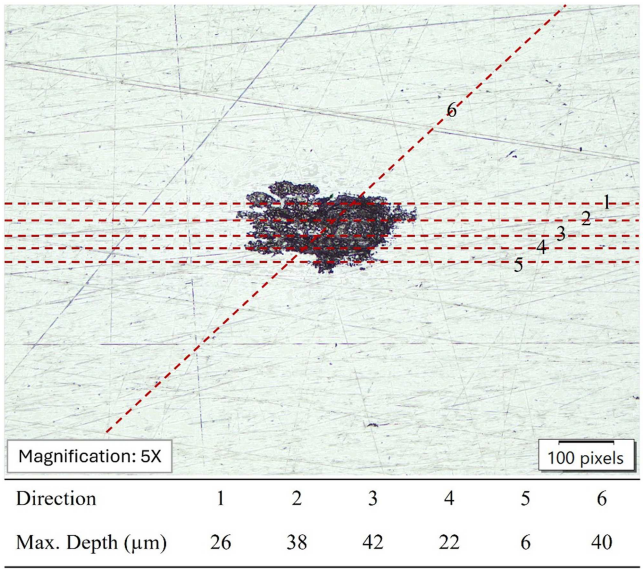

Direction	1	2	3	4	5	6
Max. Depth (μm)	26	38	42	22	6	40

FIGURE 9 | Pit depth measurements carried out by a 3D microscope on 1.4062 grade as an example. [Color figure can be viewed at wileyonlinelibrary.com]

4.2 | Crevice Test Results

4.2.1 | *Crevice Test Results for the 1.4404 Austenitic SS*

Tables 6–9 include various corrosion parameters, including the duration of active corrosion, maximum corrosion depth, corroded surface area, and enclosed area. The active corrosion duration is defined as the time interval between the initiation of localized corrosion and repassivation, that is, the recovery of the potential prior to its subsequent drop. Furthermore, the enclosed area parameter, as shown by Figure 22, represents the approximate integral of the area enclosed between the OCP curve of each specimen and that of a corrosion-free specimen. It reflects the electrochemical deviation over time and provides insight into corrosion evolution, regardless of the alloy type.

As shown in Table 6, all 1.4404 specimens exhibited corrosion; however, only four showed crevice corrosion solely. No instances of solely crevice corrosion were observed after 90 days of immersion, suggesting that pitting corrosion was the dominant mechanism and that 1.4404 is highly sensitive to it. Specimens displaying mixed corrosion modes (both pitting and crevice) are shaded in Table 6 for clarity.

Furthermore, a distinctive elongated corrosion pattern, accompanied by corrosion product deposition, was observed in 9 out of 15 specimens of grade 1.4404, as illustrated in

TABLE 6 | Data extracted from the crevice corrosion test for grade 1.4404.

Immersion time	Specimen number	Corr. type	Max. metastable corrosion duration (hour)	First active corrosion initiation (day)	Active corrosion duration (day)	Maximum corrosion depth (μm)	%Corroded area		Enclosed area (mV·day)
							First side	Second side	
35 Days	1.4404-3	Crevice	1	5	25	942	66%	49%	6.0455
	1.4404-4	Pitting + crevice	6	11	24	1047	21%	0	4.4378
	1.4404-7	Crevice	2	11	24	1702	58%	0	3.8155
	1.4404-11	Pitting + crevice	3	12	23	32	7%	0.1%	4.5693
	1.4404-12	Crevice	1	4	31	1783	73%	0	9.0479
90 Days	1.4404-2	UD + pitting + crevice	2	5	80	2333	98%	70%	14.6961
	1.4404-5	UD + pitting + crevice	3	3	87	3000	100%	100%	14.3984
	1.4404-8	Crevice	5	22	62	1627	100%	100%	12.9072
	1.4404-10	UD + crevice	1	3	62	2169	58%	0	17.1548
	1.4404-14	UD + pitting + crevice	4	26	64	1683	6%	4%	10.7496
184 Days	1.4404-1	UD + pitting + crevice	3	4	175	3000	100%	100%	35.0977
	1.4404-6	UD + pitting + crevice	10	3	181	2459	100%	100%	37.8457
	1.4404-9	UD + crevice	8	9	175	3000	100%	100%	40.0403
	1.4404-13	UD + crevice	5	76	108	3000	100%	0	14.7677
	1.4404-15	UD + crevice	4	4	180	3000	100%	90%	35.5651

Note: The shaded rows show the specimens that experienced a combination of pitting and crevice corrosion.
Abbreviation: UD, under deposition.

TABLE 7 | Data extracted from the crevice corrosion test for grade 1.4062.

Immersion time	Specimen number	Corr. type	Max. metastable corrosion duration (hour)	First active corrosion initiation (day)	Active corrosion duration (day)	Maximum corrosion depth (μm)	%Corroded area		Enclosed area (mV·day)
							First side	Second side	
35 Days	1.4062-1	Crevice	7	13	22	1091	52%	0	2.1310
	1.4062-3	Crevice	6	20	15	763	20%	0	1.3860
	1.4062-7	Crevice	8	2.5	30	1299	100%	11%	4.4420
	1.4062-10	Pitting + crevice	3	2.5	33	496	31%	0	9.6698
	1.4062-11	Pitting + crevice	12	3	32	19	3%	0	6.3569
90 Days	1.4062-2	Pitting + crevice	4	2	88	40	4%	0	17.9219
	1.4062-4	Pitting + crevice	2	2	88	96	54%	0	27.1083
	1.4062-5	Crevice	19	20	70	4000	100%	100%	19.5587
	1.4062-12	Crevice	4	20	70	1941	100%	0	11.4725
	1.4062-14	Pitting + crevice	16	16	74	1943	100%	89%	22.1273
184 Days	1.4062-6	Pitting	—	6	180	—	0	0	78.4069
	1.4062-8	Pitting + crevice	11	2	182	618	18%	0	76.5026
	1.4062-9	Pitting	1	3	181	—	0	0	59.6076
	1.4062-13	Crevice	11	3	181	2299	100%	0	63.8296
	1.4062-15	Crevice	30	144	40	1194	64%	0	9.8446

Note: The shaded rows show the samples that experienced a combination of pitting and crevice corrosion.

TABLE 8 | Data extracted from the crevice corrosion test for grade 1.4462.

Immersion time	Specimen number	Corr. type	Max. metastable corrosion duration (hour)	First active corrosion initiation (day)	Active corrosion duration (day)	Maximum corrosion depth (μm)	%Corroded area		Enclosed area (mV·day)
							First side	Second side	
35 Days	1.4462-2	Crevice	5	—	—	9	0.8%	0	0.0578
	1.4462-7	Crevice	3	—	—	6	0.3%	0	0.0260
	1.4462-8	No corrosion	3	—	—	—	—	—	—
	1.4462-11	Crevice	5	13	13	249	12%	0	0.5028
	1.4462-14	Crevice	—	16	7	117	3%	0	0.2437
90 Days	1.4462-3	Crevice	—	40	2	17	3%	0	0.0307
	1.4462-4	Crevice	—	8	6	26	2%	0	0.0059
	1.4462-6	Crevice	3	48	42	327	4%	0	1.1350
	1.4462-9	Crevice	2	38	43	280	16%	0	1.2815
	1.4462-12	Crevice	4	8	62	443	28%	18%	1.7307
184 Days	1.4462-1	Crevice	5	—	—	22	10%	0	0.0062
	1.4462-5	Crevice	1	—	—	32	8%	0	0.0197
	1.4462-10	Crevice	6	—	—	15	2%	0	0.0621
	1.4462-13	Crevice	1	114	4	36	8%	0	0.0347
	1.4462-15	No corrosion	3	—	—	—	—	—	—

Note: The shaded rows show the samples for which crevice corrosion did not occur.

TABLE 9 | Data extracted from the crevice corrosion test for 1.4410 grade.

Immersion time	Specimen number	Corr. type	Max. metastable corrosion duration (hour)	First active corrosion initiation (day)	Active corrosion duration (day)	Maximum corrosion depth (μm)	%Corroded area		Enclosed area (mV·day)
							First side	Second side	
184 Days	1.4410-1	No corrosion	4	—	—	—	—	—	—
	1.4410-2	Crevice	4	82	102	263	33%	0	12.53
	1.4410-3	No corrosion	9	—	—	—	—	—	0.42
	1.4410-4	No corrosion	6	—	—	—	—	—	0.37
	1.4410-5	Crevice	6	44	140	717	55.9%	0	16.98

Note: The shadowed rows show the samples for which the crevice corrosion did not occur.

Figure 10. The associated corrosion mechanism for this pattern is discussed further in Section 3.

As shown in Figure 11, 12 out of 15 specimens of the 1.4404 grade, specifically specimens 1.4404-1, -2, -3, -5, -6, -7, -8, -9, -10, -12, -13, and -15, have at least one side with 100% corrosion coverage. Among these, six specimens (1.4404-1, -5, -6, -8, -9, and -15) exhibited 100% corrosion coverage on both sides. Furthermore, as shown in Table 6, five specimens (1.4404-1, -5, -9, -13, and -15) were perforated through their entire thickness, indicating a high degree of degradation under the tested conditions.

After completing the crevice test, a microstructural analysis of the corroded specimens was carried out. Figure 12 shows a representative micrograph of the 1.4404 grade indicating uniform corrosion attack within the crevice region.

4.2.2 | *Crevice Test Results for the 1.4062 Lean DSS*

As shown in Table 7, all 1.4062 specimens exhibited corrosion, with no corrosion-free cases identified. A notable finding in the crevice corrosion results of 1.4062 is that 8 out of 15 specimens showed pitting corrosion, either independently or in conjunction with crevice corrosion. These pitting sites were located primarily along the cut edges. Specimens exhibiting both corrosion forms are shaded in Table 7 and were excluded from further crevice corrosion analysis, as they do not represent crevice corrosion conditions solely.

Compared with grade 1.4404, more cases of solely crevice corrosion were observed in grade 1.4062, that is, seven samples versus four. Moreover, solely crevice corrosion was observed even after 184 days of immersion for specimens 1.4062-13 and -15, and no sign of elongated corrosion, as shown in Figure 10, was detected.

As shown in Figure 13, all 1.4062 samples exhibited visible signs of corrosion in the crevice region, with varying degrees of severity. No corrosion-free samples were observed. Notably, several samples, including samples 1.4062-5, -7, -12, -13, -14, and -15, showed nearly 100% corrosion coverage on one side. Among them, samples 1.4062-5 and 1.4062-14 exhibited complete corrosion coverage on both sides. Furthermore, specimen 1.4062-5 experienced through-thickness perforation. Even without detailed numerical analysis, a visual comparison between Figures 11 and 13 suggests a more noble crevice corrosion behavior for 1.4062 than 1.4404.

According to Figure 14, corrosion of both ferrite and austenite phases can be observed simultaneously in the crevice region of the corroded 1.4062 samples.

4.2.3 | *Crevice Test Results for the 1.4462 Standard DSS*

Table 8 summarizes all the measured parameters from the crevice corrosion tests conducted on 1.4462. As shown, two samples, 1.4462-8 and 1.4462-15, remained corrosion-free after 35 and 184 days of exposure, respectively. These samples are shaded in Table 8 for easy identification. The remaining 13 samples exhibited signs of crevice corrosion. Among them, seven showed only metastable potential drops without progression to active corrosion.

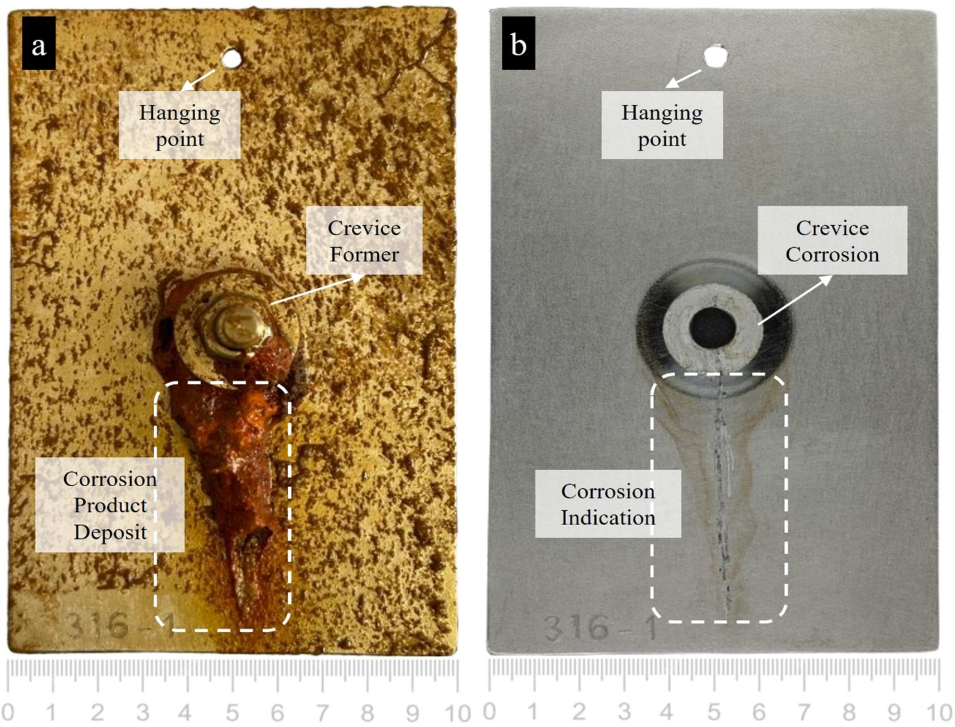

FIGURE 10 | 1.4404 austenitic SS specimen no. 1.4404-1: (a) before cleaning and (b) after cleaning. [Color figure can be viewed at wileyonlinelibrary.com]

Notably, specimen 1.4462-5 displayed an unusual corrosion pattern, where initiation did not occur at the crevice edge. Two classical theories explain the crevice corrosion initiation: the critical crevice solution theory (CCST) and the IR drop theory (IRDT) [2, 51–54]. Considering the IRDT, the crevice should be initiated in the vicinity of the crevice entrance/mouth. All 1.4462 samples followed this theory except for sample 1.4462-5. Therefore, owing to its atypical behavior, it was excluded from further corrosion assessments. Analysis of the six remaining samples suggested that a continuous potential drop of at least 5 h was required to produce a visible surface indication.

According to Figure 15, all samples except 1.4462-8 and 1.4462-15 exhibited visible corrosion indications in the crevice region. However, the severity of corrosion varies significantly among the affected samples. Compared with 1.4404 and 1.4062, both the number of corroded samples and the severity of corrosion in the 1.4462 samples are significantly lower.

Figure 16 shows that, similar to 1.4062, corrosion occurred in both the ferrite and austenite phases, depending on the inspection location within the crevice profile.

4.2.4 | Crevice Test Results for the 1.4410 Super DSS

Table 9 presents the crevice corrosion test results for alloy 1.4410. Among the five tested samples, three remained corrosion-free after 184 days of exposure to natural seawater at 20°C. These non-corroded specimens are shaded in Table 9 for clarity. Conversely, two samples exhibited signs of corrosion. The enclosed area parameters obtained for the corroded samples of 1.4410-1, -3, and -4 are consistent with the suggestion in Section 4.2.3 that a continuous potential drop of at least 5 h is required to initiate corrosion.

An evaluation of the OCP trends is shown in Figure 17. The initial OCP oscillations occurring during the first weeks are attributed to the metastable pits in the cut edges. The results reveal that the three non-corroded specimens experienced only metastable potential drops, indicating the absence of active corrosion. Among these samples, specimen 1.4410-1, which exhibited a maximum metastable potential drop lasting less than 4 h, remained completely free of discoloration. The other two samples, 1.4410-3 and 1.4410-4, experienced longer metastable potential drops of 9 and 6 h, respectively, and displayed some surface discoloration, but no measurable corrosion.

In contrast, samples 1.4410-2 and 1.4410-5 (the corroded samples) exhibited significant and sustained decreases in potential, clearly indicating the initiation of active crevice corrosion. After 184 days, this led to maximum corrosion depths of 263 and 717 μm, as shown in Table 9, for samples 1.4410-2 and 1.4410-5, respectively.

Figure 18 shows the crevice zones on both sides of all five samples, including the two corroded (1.4410-2 and 1.4410-5) and three non-corroded (1.4410-1, 1.4410-3, and 1.4410-4) samples. Compared to the grade 1.4462 sample, a lower percentage of the samples were corroded (40% vs. 87%).

Figure 19 presents micrographs of the corroded surface of the 1.4410 grade. As shown, simultaneous corrosion of both ferrite and austenite was observed. This feature was also previously observed in the 1.4462 and 1.4062 DSS grades.

5 | Discussion

In terms of pitting resistance, the CPT results confirmed the PREN-derived ranking: 1.4410 > 1.4462 > 1.4062 > 1.4404. This ranking was further supported by the crevice immersion test. In the cases of 1.4410 and 1.4462, no pitting was observed, interfering with crevice

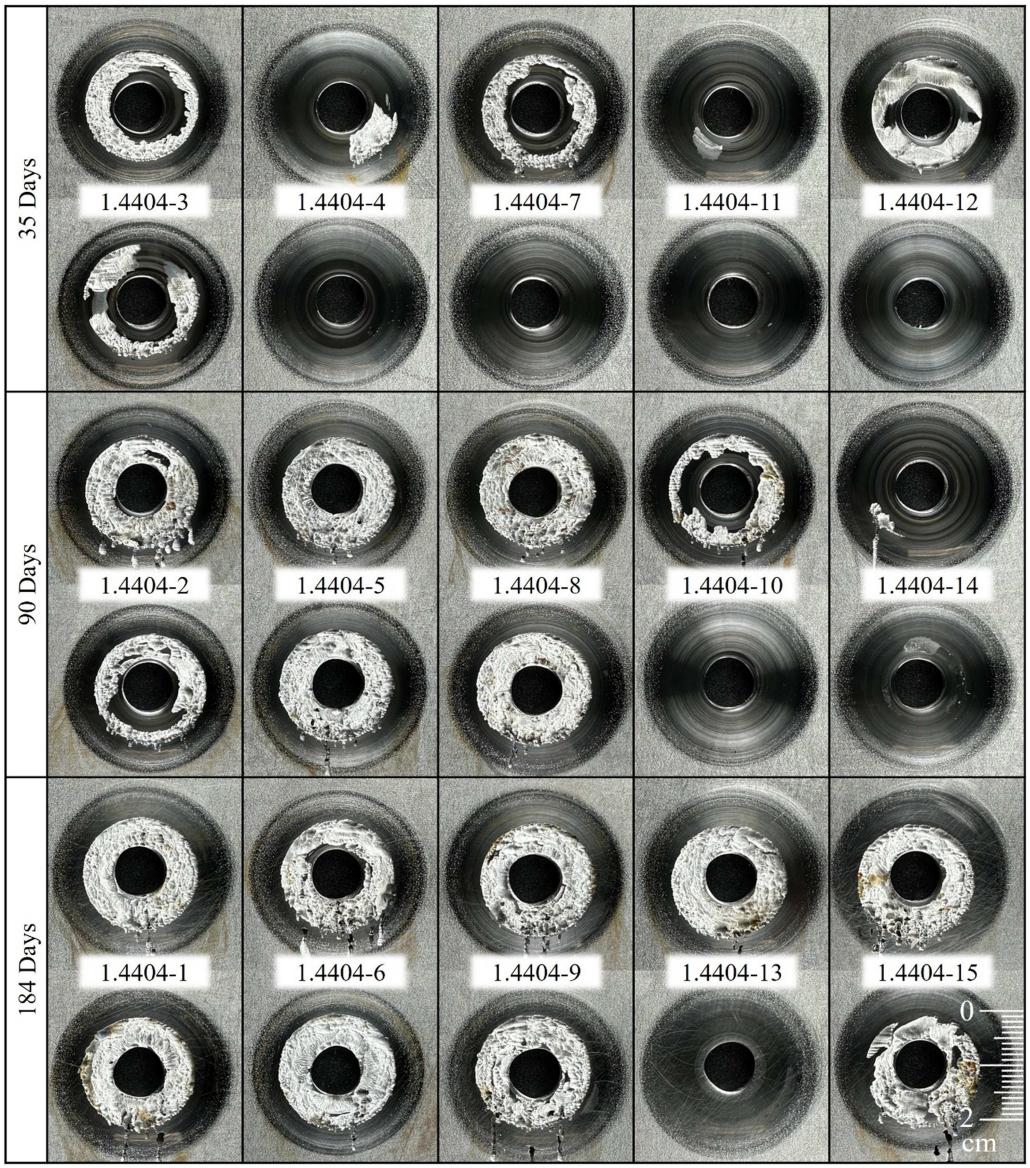

FIGURE 11 | Macro-photos taken from the crevice regions of both sides for the 1.4404 specimens.

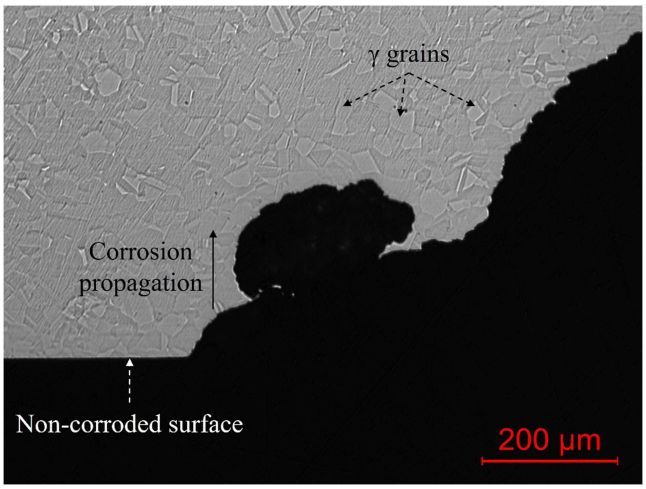

FIGURE 12 | Micrograph of the corroded surface of 1.4404 sample by OM. [Color figure can be viewed at wileyonlinelibrary.com]

corrosion. In contrast, pitting occurred in 8 out of 15 samples and in 11 out of 15 samples for 1.4062 and 1.4404, respectively. Notably, two 1.4062 samples remained pitting-free even after 184 days of exposure, whereas all 1.4404 samples exhibited pitting within 90 days of exposure.

Moreover, pitting in the 1.4062 samples was limited to the sample edges. However, for 1.4404, an additional form of corrosion was observed under corrosion deposits. In the literature, it has been referred to as elongated pitting [55]. This phenomenon is explained by the critical crevice solution theory (CCST), which states that the crevice former creates an oxygen concentration cell, with the crevice region acting as the anodic area and the surrounding oxygen-rich region acting as the cathodic area. Within the crevice, the lack of oxygen reduction allows the accumulation of metal cations from anodic dissolution, which attracts chloride ions and generates a concentrated acidic solution via hydrolysis [2, 56]. Due to its high specific gravity, this solution flows downward under gravity, breaking down the passive layer upon contact with the surface.

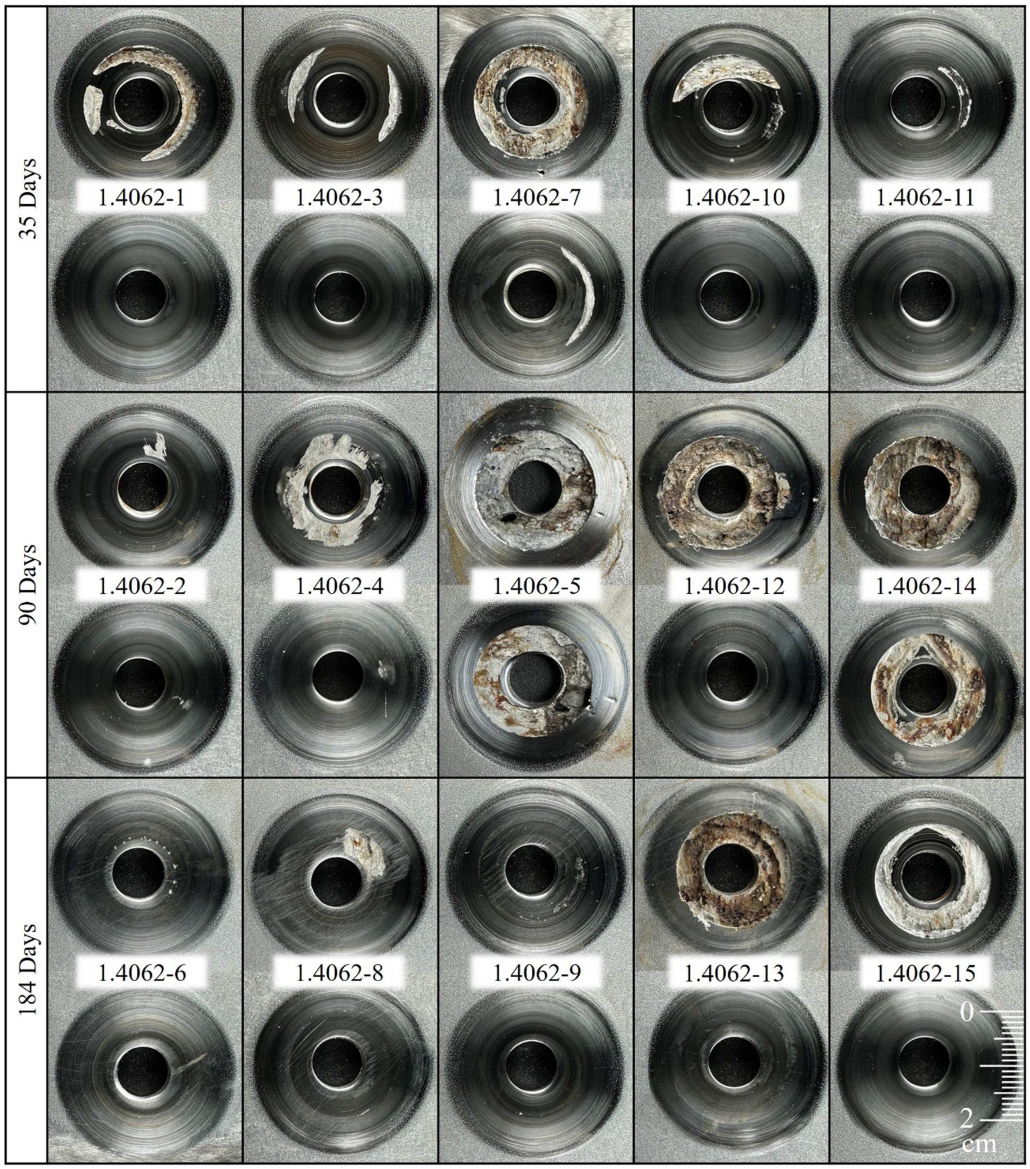

FIGURE 13 | Macro-photos taken from the crevice regions of both sides for the 1.4062 samples. [Color figure can be viewed at wileyonlinelibrary.com]

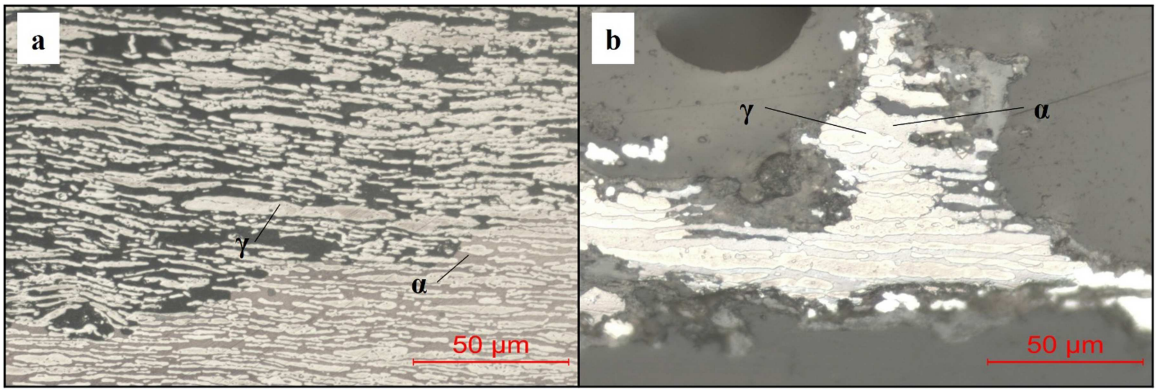

FIGURE 14 | Micrographs of the corroded surface of grade 1.4062. (a) Corrosion of ferrite (α). (b) Corrosion of austenite (γ). [Color figure can be viewed at wileyonlinelibrary.com]

This mechanism accounts for the elongated corrosion features observed in the 1.4404 samples, all of which originated from the lower edge of the crevice former and extended downward (Figure 10). Whereas this feature was absent in the samples removed from the test medium after 35 days of exposure, it was observed in almost all samples retrieved after 90 and 184 days. This suggests that a minimum duration was required to form highly corrosive condition below corrosion deposit. The absence

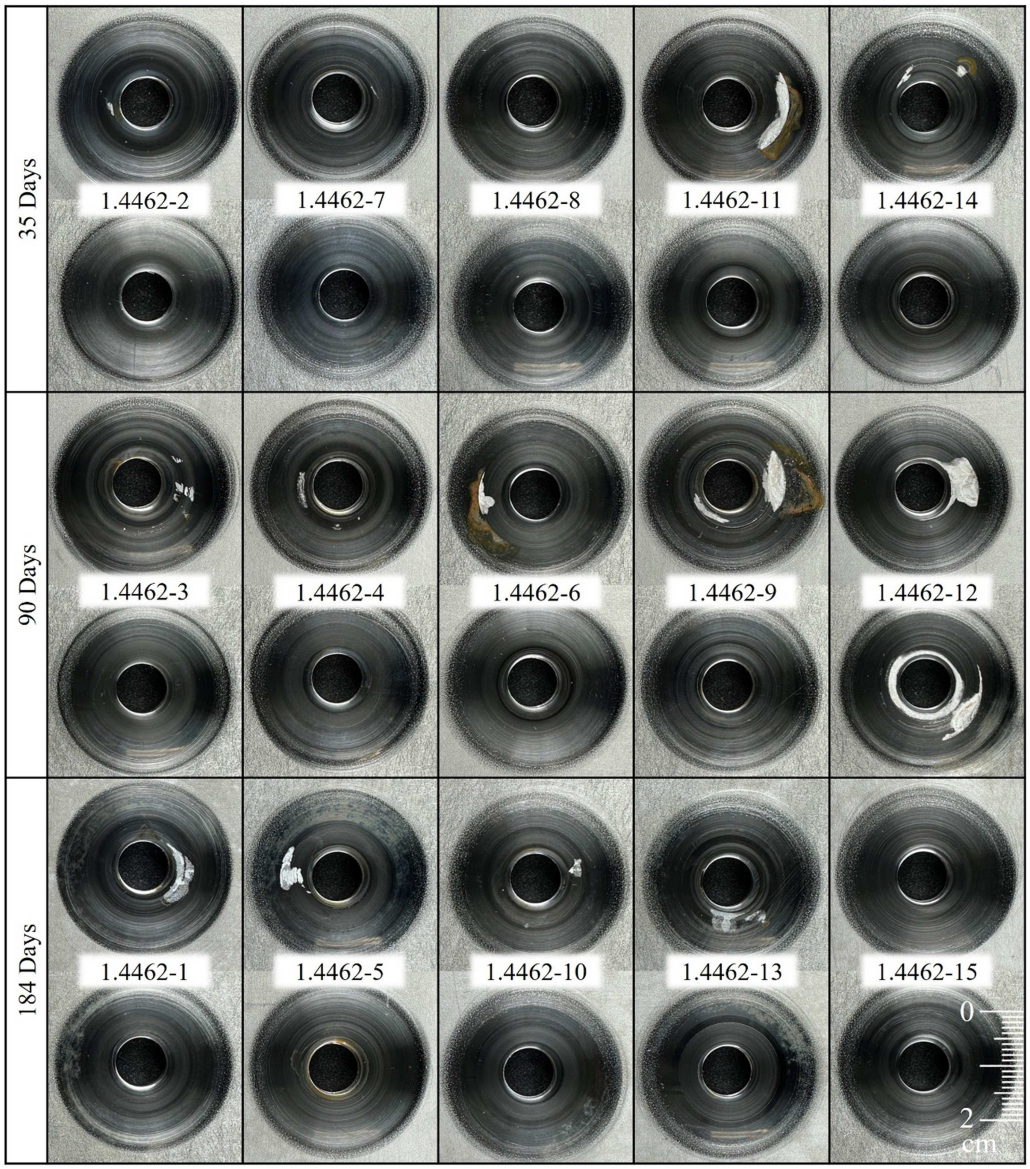

FIGURE 15 | Macro-photos taken from the crevice regions of both sides for the 1.4462 samples. [Color figure can be viewed at wileyonlinelibrary.com]

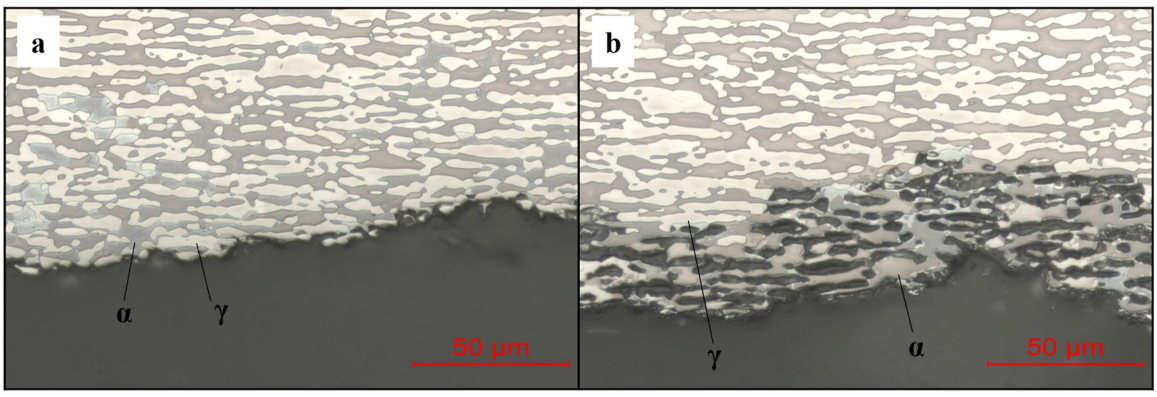

FIGURE 16 | Micrographs of the corroded surface of grade 1.4462. (a) Corrosion of ferrite (α). (b) Corrosion of austenite (γ). [Color figure can be viewed at wileyonlinelibrary.com]

of such corrosion in the 1.4062 samples implies that its passive film offers greater resistance to acidic environments, making 1.4062 a safer alternative to 1.4404 in conditions susceptible to this type of localized corrosion.

Regarding crevice corrosion, on the basis of the results presented in Tables 6–9 and Figures 11, 13, 15, and 18, none of the materials evaluated in this study were fully resistant to crevice corrosion. Even super DSS and standard DSS exhibited varying

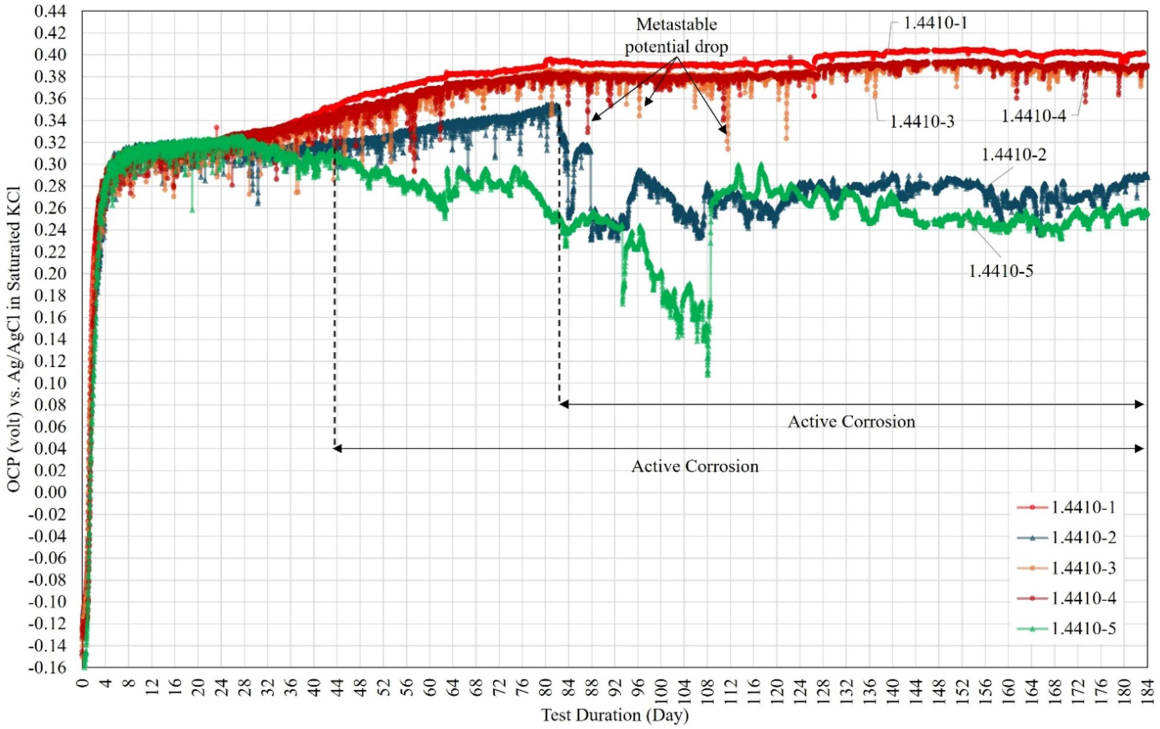

FIGURE 17 | OCP trends of five 1.4410 samples, including 1.4410-1, 1.4410-2, 1.4410-3, 1.4410-4, and 1.4410-5, for 184 days of immersion in natural seawater at ambient temperature (20°C) and under 20 N/mm^2 pressure. [Color figure can be viewed at wileyonlinelibrary.com]

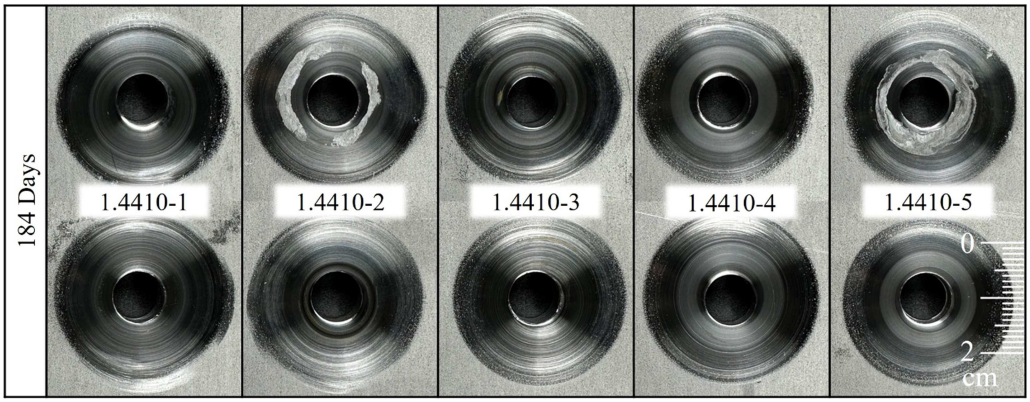

FIGURE 18 | Macro-photos taken from the crevice regions of both sides for the 1.4410 samples.

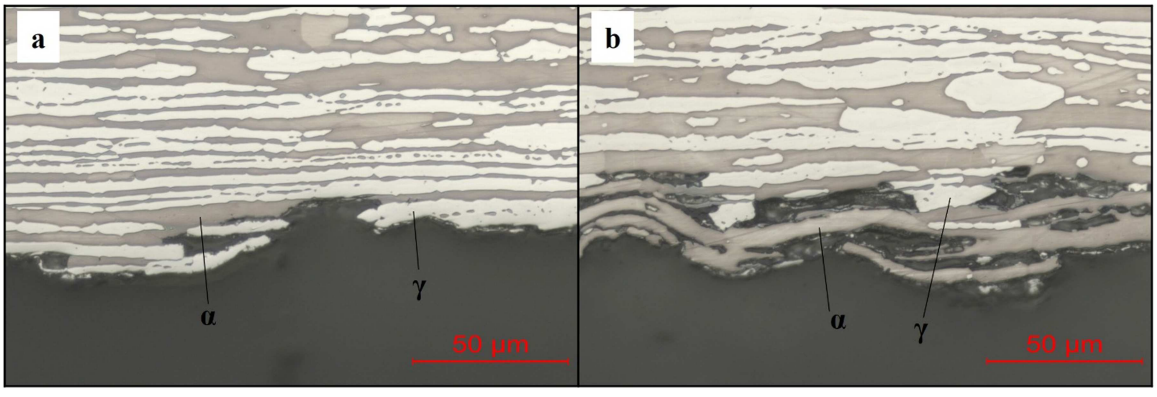

FIGURE 19 | Micrographs of the corroded surface of grade 1.4410. (a) Corrosion of ferrite (α). (b) Corrosion of austenite (γ). [Color figure can be viewed at wileyonlinelibrary.com]

degrees of attack. This observation suggests that, although some studies [5–7, 13, 43] have shown that super DSSs exhibit resistance to crevice corrosion in seawater at 20°C, altering the crevice conditions, for example, increasing the severity of the geometry, can significantly affect their performance. For example, although this study uses the same test temperature (20°C), test medium (natural seawater from Brest Bay, France), and applied pressure (20 N/mm^2) as those used in Larché [44], the significantly lower surface roughness used here (0.3 μm compared with 3 μm in Larché's study) is known to promote more aggressive crevice conditions [21].

Despite the occurrence of crevice corrosion in all four tested grades, its extent and severity varied. As shown in Table 10, none of the 1.4410 or 1.4462 samples experienced complete (100%) corrosion within the crevice region. In contrast, both 1.4062 and 1.4404 presented cases of full crevice zone corrosion, with the incidence being significantly greater for 1.4404. Specifically, the number of samples exhibiting 100% corrosion on at least one side was 1.6 times greater for 1.4404 than for 1.4062. Accordingly, on the basis of the corroded area parameter, the crevice corrosion resistance ranking is confirmed as follows: 1.4410 > 1.4462 > 1.4062 > 1.4404.

Figure 20 shows the distribution of corrosion depth for the four grades after 35 days of immersion in natural seawater. Among the tested materials, the 1.4404 grade exhibited the highest average and median of corrosion depths, along with the largest variation, indicating a less consistent corrosion resistance performance. In contrast, the 1.4062 grade demonstrated a lower average, median, and variation in corrosion depth, suggesting more stable behavior, although still inferior to that of the 1.4462 grade. As illustrated in Figure 20, the average corrosion depth of 1.4404 is approximately 1.5 times higher than that of 1.4062. Based on Figure 17, which shows no potential drop over 35 days, and the visual inspection of the immersed samples, no corrosion was observed on grade 1.4410 after 35 days of immersion. Thus, the previously established ranking of crevice corrosion resistance is further validated.

Figure 21 presents the OCP curves of a non-corroded standard duplex specimen (1.4462-15) and a corroded lean duplex specimen (1.4062-15). In general, OCP reflects the mixed potential of the anodic and cathodic regions on a single sample surface [57]. As sample 1.4462-15 remained free of corrosion after 184 days of immersion, its OCP behavior can be considered representative of corrosion-free conditions. Given the compositional similarities between 1.4462, 1.4062, and 1.4404, the OCP trend observed for 1.4462-15 may also serve as an approximate baseline for these grades.

Additionally, Figure 21 illustrates the different stages of OCP evolution for 1.4062-15, which serves as an example of a crevice-corroded sample. Both samples shown in Figure 21 exhibit a noble potential shift. This phenomenon, known as potential ennoblement, occurs in passive metals exposed to natural seawater and is attributed to biofilm formation on the metal surface. The biofilm enhances the cathodic reduction of oxygen through various mechanisms described in previous studies [21, 58–60]. Potential ennoblement increases the susceptibility to localized corrosion by shifting the metal's potential closer to the critical pitting and crevice corrosion potential [4]. While non-corroded specimens (e.g., 1.4462-15) show only metastable potential drops, corroded samples (e.g., 1.4062-15) exhibit significant and sustained potential drops, indicating the onset of active corrosion [11, 13, 61–63]. Consequently, the OCP curves of non-corroded specimens are used as a reference to interpret the corrosion behavior of other samples. This is similar to the method used in electrochemical noise (EN) sensors [63–65]. This method can also be used to quantify different corrosion parameters, including the corrosion initiation time. For example, in Figure 22, the OCP of specimen 1.4462-12 begins to deviate from the reference trend (non-corroded

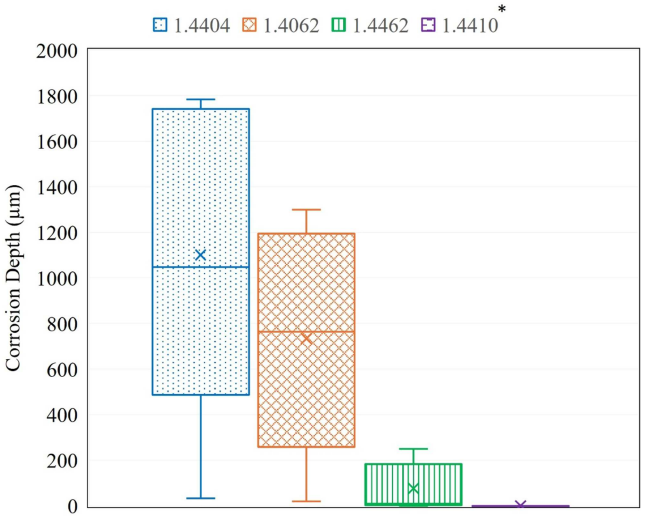

FIGURE 20 | Corrosion depth distributions for four grades: 1.4404, 1.4062, 1.4462, and 1.4410, after 35 days of immersion. The average corrosion depths are shown by cross marks on the box and whisker charts. *For grade 1.4410, no potential drop indicative of localized corrosion was observed in the OCP plots over 35 days (Figure 17), which was confirmed by the visual inspection of the immersed samples. Therefore, the corrosion depth was considered zero for this grade. [Color figure can be viewed at wileyonlinelibrary.com]

TABLE 10 | Severity of crevice corrosion for grades 1.4410, 1.4462, 1.4062, and 1.4404 considering their corroded area.

Material grade	Maximum of % corroded area	No. of one-side 100% corroded area	No. of two-side 100% corroded area
1.4410 (2507)	56%	0	0
1.4462 (2205)	46%	0	0
1.4062 (2202)	100%	5	1
1.4404 (316 L)	100%	8	5

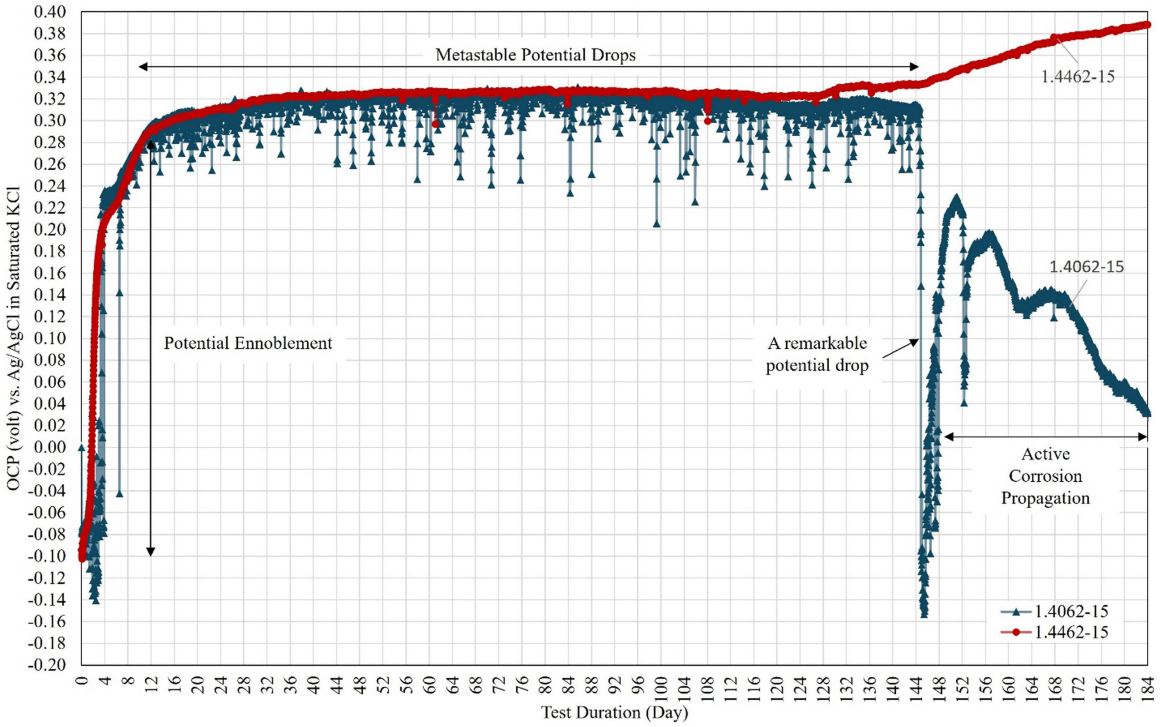

FIGURE 21 | OCP curves of a non-corroded specimen 1.4462-15 (red) and a corroded specimen 1.4062-15 (blue). [Color figure can be viewed at wileyonlinelibrary.com]

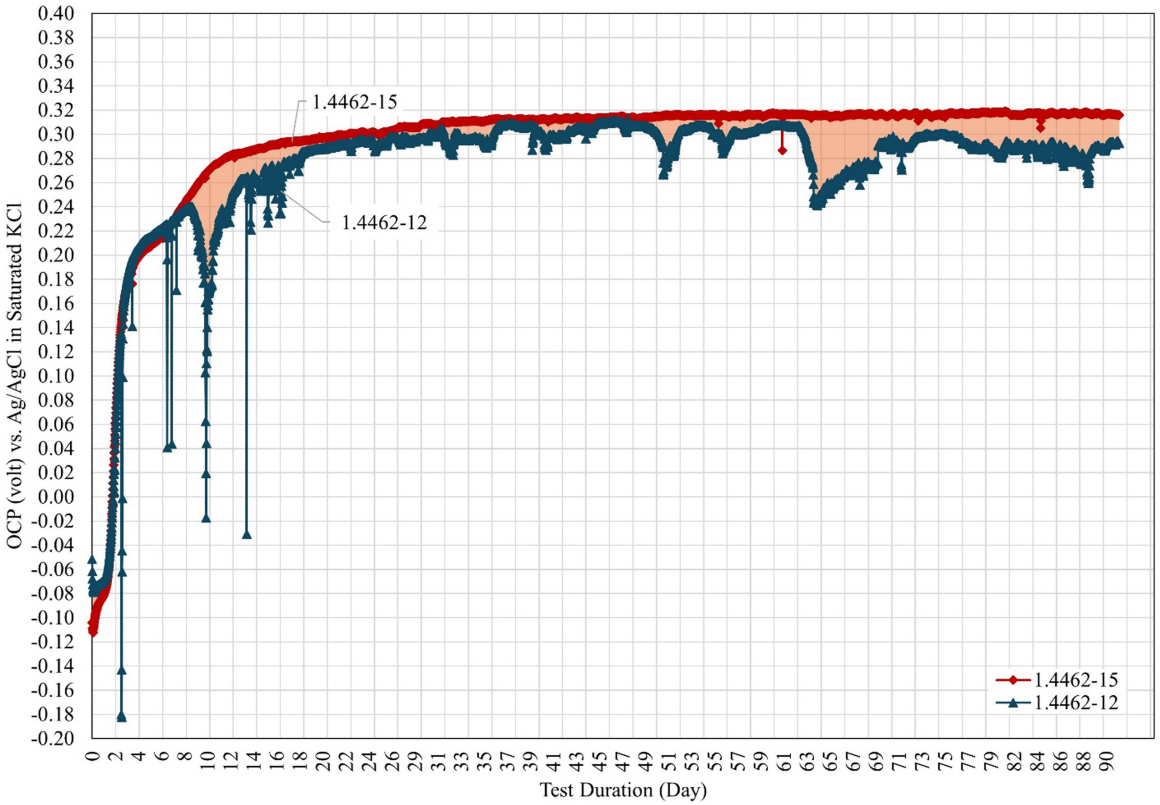

FIGURE 22 | OCP graphs of 1.4462-15 and -12 depicted in the same time range. When the blue (1.4462-12) graph deviates from the red (1.4462-15) graph, corrosion has occurred. The enclosed area has been shaded. [Color figure can be viewed at wileyonlinelibrary.com]

specimen 1.4462-15) after approximately 7 days, indicating the initiation of crevice corrosion. This deviation, entitled the enclosed area in the result tables, is shown by the shaded region in Figure 22. There is potential to correlate the empirical data of the enclosed area, corrosion depth, and corrosion duration to develop a numerical model for estimating the corrosion rate. However, further research is needed to establish and validate such a model in practical applications.

The four target grades in this study are categorized in Figure 23 based on the time to active corrosion initiation. "Active Corrosion Initiation" was determined by the first significant potential drop in the OCP graph, which lasts for at least 1 day.

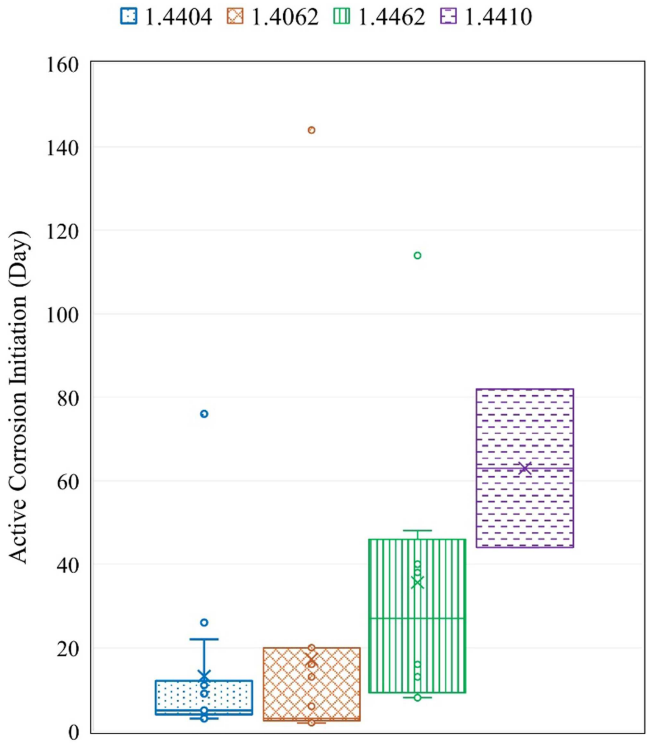

FIGURE 23 | Initiation day of active corrosion in the immersion crevice test for 1.4410, 1.4462, 1.4062, and 1.4404. [Color figure can be viewed at wileyonlinelibrary.com]

The time required for active corrosion initiation is the shortest for 1.4404, followed by 1.4062 and then 1.4462. As expected, the longest incubation time before corrosion initiation was observed at 1.4410. Substituting 1.4062 for 1.4404 could allow approximately 30% more exposure time in seawater before corrosion begins, which may be significant for applications where the system is in limited contact with seawater prior to reaching normal service conditions. Based on the time to first corrosion initiation, the tested grades can be ranked as follows: 1.4404 < 1.4062 < 1.4462 < 1.4410.

Previous studies have shown that, in the absence of secondary phases, localized corrosion in DSSs occurs as selective corrosion of either the ferrite or austenite phase [66–69]. Some studies have proposed that this process is governed primarily by the phase with lower corrosion resistance and can be correlated with the local pitting resistance equivalent (PREN) of each phase [48, 70, 71]. To evaluate the validity of this correlation, a corroded sample of 1.4462 DSS was analyzed. As shown in Figure 24, energy-dispersive spectroscopy (EDS) was performed on both the austenite and ferrite phases to determine their chemical compositions and to calculate their local PREN values via Equation (1). Notably, owing to the limitations of EDS in measuring nitrogen content, an established method from the literature was adopted for its estimation [71].

According to Table 11, the PREN values of the ferrite phase are significantly higher than those of the austenite phase, which would theoretically suggest superior resistance to localized corrosion. However, as shown in Figure 24, selective corrosion occurred in the ferrite phase within this region of the sample. This observation challenges the assumption that local PREN values alone are sufficient to predict the selective corrosion behavior between the ferrite and austenite phases and that the

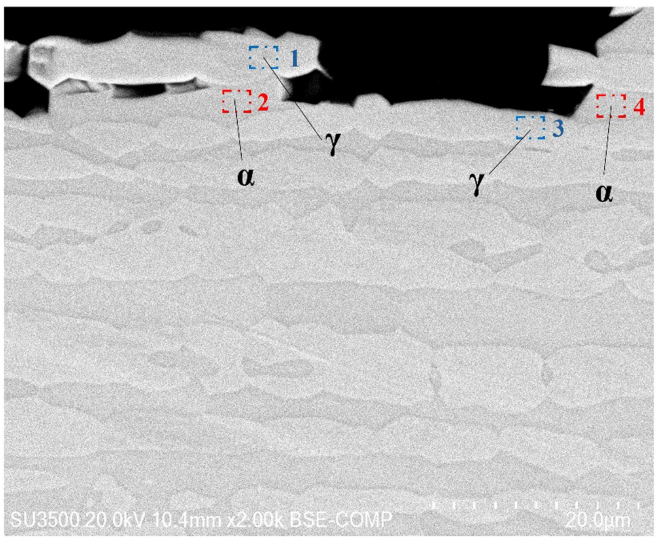

Sampling	Cr (%wt)	Mo (%wt)	N (%wt)	Ni (%wt)
Point 1 (γ)	21.80	2.70	0.32	6.90
Point 2 (α)	25.40	3.90	0.05	3.60
Point 3 (γ)	21.90	2.20	0.05	6.70
Point 4 (α)	25.10	3.90	0.32	4.40

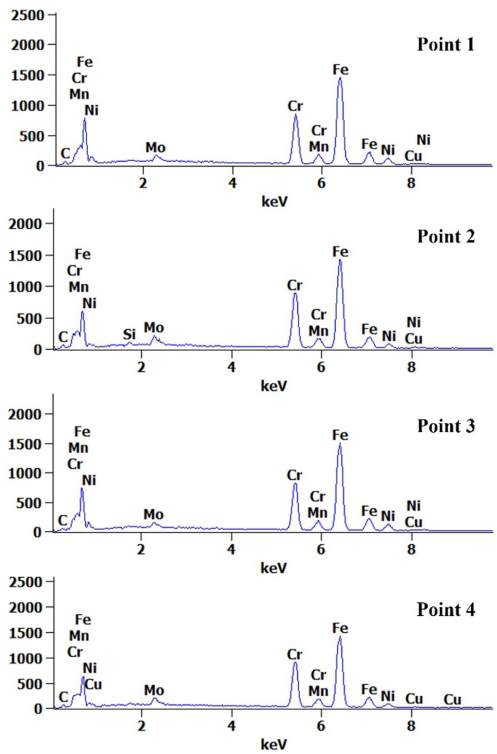

FIGURE 24 | EDS analysis of the ferrite and austenite phases in a 1.4462 DSS sample, close to the corroded zone. [Color figure can be viewed at wileyonlinelibrary.com]

solution they are exposed to, and its pH should also be considered.

Several studies [2, 21, 22, 43, 48, 66] have reported the selective corrosion of the ferrite phase in DSSs when they are exposed to natural seawater, chlorinated seawater, and wastewater. Moreover, other works [67–69, 72] indicate that the preferentially corroded phase may vary depending on both the metallurgical characteristics of the material and the properties of the corrosive environment. Tsai et al. [67] proposed that the nature of the oxidizing anions, in addition to the chemical composition of the alloy, governs the corrosion behavior of ferrite and austenite. They demonstrated that in a H_2SO_4+HCl solution, the ferrite phase in 1.4462 DSS acts as the anode and is selectively corroded. In contrast, in HNO_3 solution, austenite becomes the anodic phase and is preferentially corroded. This behavior is attributed to the partitioning of alloying elements between the ferrite and austenite

TABLE 11 | PREN of two ferrite phases and two austenite phases close to the corroded surface of the 1.4462 sample.

Sampling point	Point 1 (γ)	Point 2 (α)	Point 3 (γ)	Point 4 (α)
PREN	35.7	39.1	34.2	38.8

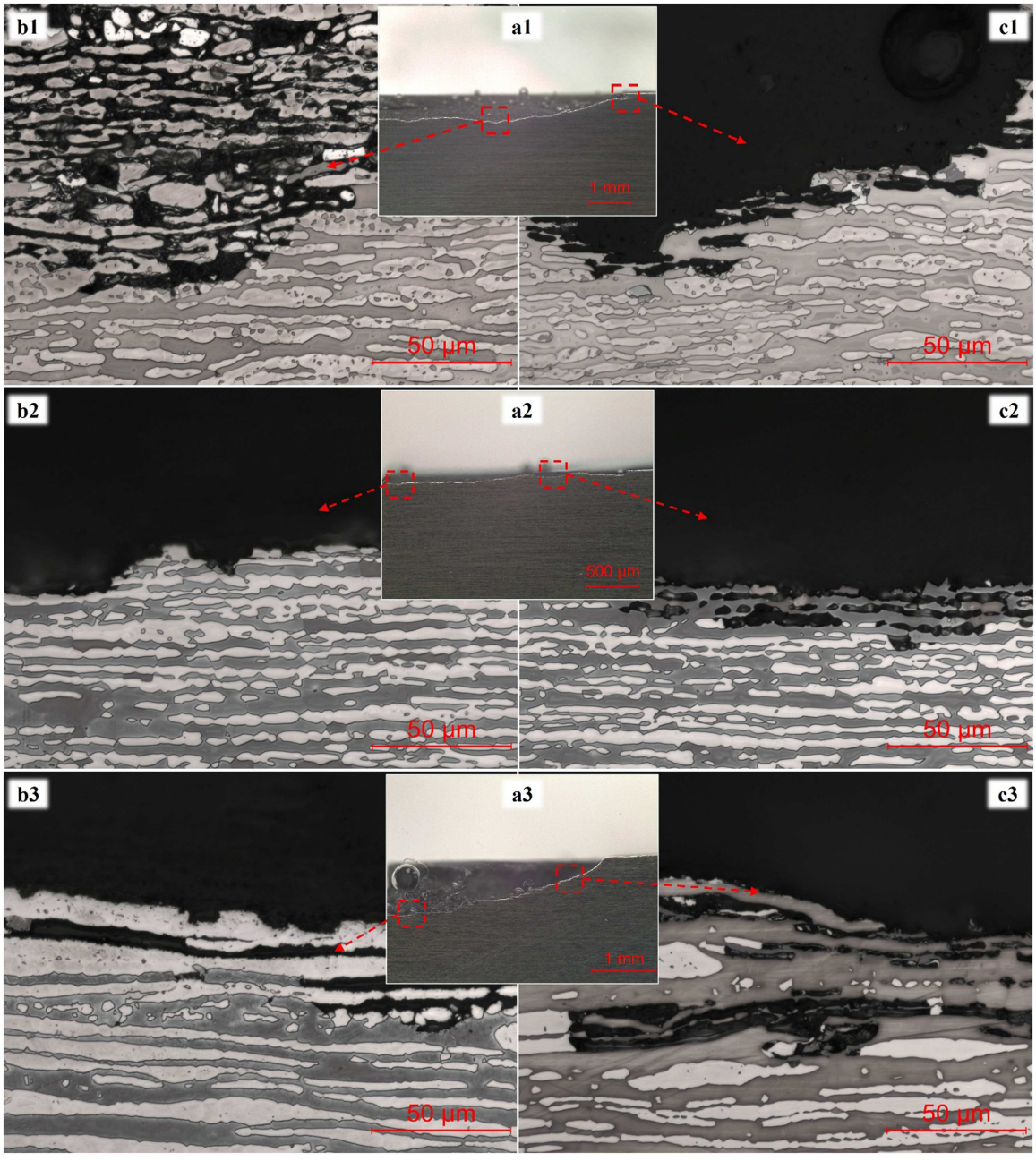

FIGURE 25 | (a1), (a2), (a3) Binocular images from the cross-sectional view of the corrosion profile at 1.4062, 1.4462, and 1.4410, respectively. (b1), (b2), (b3) Corrosion in ferrite (α) for 1.4062, 1.4462, and 1.4410, respectively. (c1), (c2), (c3) Corrosion in austenite (γ) for 1.4062, 1.4462, and 1.4410, respectively. [Color figure can be viewed at wileyonlinelibrary.com]

phases, which causes their corrosion responses to differ in various environments [67–69, 72].

In the present study, as illustrated in Figures 14, 16, and 19, corrosion of both the ferrite and austenite phases occurred simultaneously across all three examined DSS grades. This observation is consistent with the findings of Ruel et al. [73], who proposed that selective phase corrosion is influenced not only by the alloy composition of the material and the oxidizing power of the solution but also by the local pH. As such, in different surface regions of the same material, where the pH may vary, selective corrosion can manifest in different phases. Ruel et al. [73] demonstrated that in 1.4362 lean DSS exposed to NACE TM0177 solution, austenite corrodes preferentially at the early stage. As acidification progresses, particularly at the bottom of a defect, ferrite corrosion ensues. In the present study, the observed correlation between corrosion mechanisms and their spatial locations aligns well with Ruel's findings. As shown in Figure 25, corrosion of both phases is evident across all three DSS grades. Specifically, austenite (γ) preferentially corroded near the surface, whereas ferrite (α) exhibited greater corrosion deeper within the profile, where the local environment is likely more acidic. Therefore, no evidence of the selective corrosion of a specific phase was observed.

6 | Conclusion

In this study, the localized corrosion behavior of grades 1.4404, 1.4062, 1.4462, and 1.4410 was evaluated via CPT electrochemical tests, crevice immersion tests, and OCP monitoring. To assess corrosion severity and mechanism, as well as to identify the corroded phase, corrosion depth, and corrosion profile, a combination of 3D microscopy, SEM, EDS, optical microscopy (OM) with the focalization method, and VSI microscopy was employed. By combining these electrochemical and microscopic techniques across four widely used stainless steel grades, our study provides a detailed assessment of localized corrosion behavior and draws important conclusions regarding material selection in seawater.

The following conclusions were drawn:

- The CPT test results and the results from the crevice immersion tests confirm the ranking of localized corrosion resistance for the four studied grades as follows: $1.4404 < 1.4062 < 1.4462 < 1.4410$.
- Various measured crevice parameters, including the active corrosion initiation day, corroded area, and corrosion depth, validate the crevice corrosion resistance of the four studied grades, with the same ranking.
- The crevice tests revealed that under severe crevice conditions, as used in this study, all tested grades experienced corrosion after 6 months at 20°C when subjected to a crevice geometry of $20\,N/mm^2$ pressure and $0.3 \pm 0.1\,\mu m$ surface roughness.
- The 1.4062 grade proves to be a cost-effective option for applications involving limited contact with seawater before normal service conditions are established. Its resistance to both pitting and crevice corrosion is approximately 1.3 times greater than that of 1.4404.
- Simultaneous corrosion of austenite and ferrite in seawater may occur, with a greater probability of austenite being preferentially corroded near the surface and in shallow crevices, whereas ferrite is more susceptible to corrosion near the bottom and in deeper crevices, where the pH is lower.
- The local PREN of ferrite and austenite does not reliably predict the preferential phase for selective corrosion.
- Additionally, this study demonstrates that using the OCP graph of a non-corroded specimen as a baseline allows deviations to be monitored over time. Analyzing deviations from this baseline graph would provide a reliable method for early corrosion detection and quantitative rate estimation. This methodology could serve as a practical tool for continuous monitoring of key stainless steel structures in seawater.

Author Contributions

Mohammad Hassanzadeh: conceptualization, data curation, methodology, formal analysis, investigation, writing – original draft, visualization. **Nicolas Larché:** conceptualization, methodology, writing – review and editing, supervision, resources, validation, project administration, funding acquisition. **Audrey Allion-Maurer:** conceptualization, writing – review and editing, resources, project administration. **Raf Dewil:** conceptualization, writing – review and editing, supervision, funding acquisition. **Barbara Rossi:** conceptualization, writing – review and editing, supervision.

Acknowledgments

The authors gratefully acknowledge the valuable support provided by the technicians and engineers at French Corrosion Institute and APERAM company. Their assistance with technical guidance and practical expertise was essential for the successful completion of this study. This study was funded by the European Union (Horizon Europe Marie Skłodowska-Curie Actions Grant Agreement No. 101073471). The views and opinions expressed are, however, those of the authors only and do not necessarily reflect those of the European Union or the European Research Executive Agency. Neither the European Union nor the granting authority can be held responsible for them.

Data Availability Statement

The original contributions presented in the study are included in the article/supporting information; further inquiries can be directed to the corresponding author.

References

1. B. Kan, W. Wu, Z. Yang, X. Zhang, and J. Li, "Effects of Hydrostatic Pressure and pH on the Corrosion Behavior of 2205 Duplex Stainless Steel," *Journal of Electroanalytical Chemistry* 886 (2021): 115134, https://doi.org/10.1016/J.JELECHEM.2021.115134.

2. Z. Zhang, Z. Li, F. Wu, et al., "A Comparison Study of Crevice Corrosion on Typical Stainless Steels Under Biofouling and Artificial Configurations," *npj Materials Degradation* 6 (2022): 85, https://doi.org/10.1038/s41529-022-00301-w.

3. X. Chen, C. Xiao, X. Wang, J. Yang, and C. He, "Corrosion Behaviors of 2205 Duplex Stainless Steel in Biotic and Abiotic NaCl Solutions," *Construction and Building Materials* 342 (2022): 127699, https://doi.org/10.1016/j.conbuildmat.2022.127699.

4. D. A. Fischer, L. Daille, J. Aguirre, et al., "Corrosion of Stainless Steel in Simulated Tide of Fresh Natural Seawater of South East Pacific,"

International Journal of Electrochemical Science 11 (2016): 6873–6885, https://doi.org/10.20964/2016.08.50.

5. N. Larché, E. Diler, and D. Thierry, "Crevice and Pitting Corrosion of Stainless-Steel and Nickel Based Alloys in Deep Sea Water," paper presented at Corrosion 2019, Nashville, TN, March 24–28, 2019 (NACE International, 2019), https://doi.org/10.5006/C2019-13123.

6. "ISO 21457 Standard: Materials Selection and Corrosion Control for Oil and Gas Production Systems," ISO, 2010, https://www.iso.org/standard/45938.html.

7. "NORSOK M-001: Materials Selection Standard," Standards Norway, 2014, https://online.standard.no/en/norsok-m-001-2014.

8. "The Stainless Steel Family," International Stainless Steel Forum (ISSF), 2019, https://worldstainless.org/about-stainless/properties/stainless-steel-standards/.

9. K. R. Larsen, "Selecting Stainless Steels for Seawater Pumps," *Materials Performance* 55 (2016): 28–32, https://content.ampp.org/materials-performance/magazine-article/2291/Selecting-Stainless-Steels-for-Seawater-Pumps?searchresult=1.

10. J. P. Audouard and M. Verneau, "Highly Alloyed Stainless Steels for Sea Water Applications," paper presented at Corrosion 1996, Denver, CO, March 24–29, 1996 (NACE International, 1996), https://doi.org/10.5006/C1996-96508.

11. H. Zeng, Y. Yang, L. Liu, and M. Li, "Pitting and Crevice Corrosion Evolution Characteristics of 2205 Duplex Stainless Steel in Hot Concentrated Seawater," *Journal of Solid State Electrochemistry* 25 (2021): 1555–1565, https://doi.org/10.1007/s10008-021-04935-9.

12. J. Zhu, D. Li, W. Chang, et al., "In Situ Marine Exposure Study on Corrosion Behaviors of Five Alloys in Coastal Waters of Western Pacific Ocean," *Journal of Materials Research and Technology* 9 (2020): 8104–8116, https://doi.org/10.1016/J.JMRT.2020.05.060.

13. E. B. Haugan, M. Næss, C. T. Rodriguez, R. Johnsen, and M. Iannuzzi, "Effect of Tungsten on the Pitting and Crevice Corrosion Resistance of Type 25Cr Super Duplex Stainless Steels," *Corrosion* 73 (2016): 53–67, https://doi.org/10.5006/2185.

14. "Duplex Stainless Steels, Brussels," International Stainless Steel Forum, 2021, https://worldstainless.org/.

15. "A Practical Guide to Duplex Stainless Steels (10044)," Nickle Institute, 2021, https://nickelinstitute.org/en/resources/technical-guides/a-practical-guide-to-duplex-stainless-steels-10044/.

16. "NORSOK M-630: Material Data Sheets and Element Data Sheets for Piping," Standards Norway, 2020, https://online.standard.no/en/norsok-m-630-2020.

17. M. E. Wilms, V. J. Gadgil, J. M. Krougman, and F. P. Ijsseling, "The Effect of σ-Phase Precipitation at 800°C on the Corrosion Resistance in Seawater of a High Alloyed Duplex Stainless Steel," *Corrosion Science* 36 (1994): 871–881, https://doi.org/10.1016/0010-938X(94)90176-7.

18. H. M. Ezuber, A. El-Houd, and F. El-Shawesh, "Effects of Sigma Phase Precipitation on Seawater Pitting of Duplex Stainless Steel," *Desalination* 207 (2007): 268–275, https://doi.org/10.1016/J.DESAL.2006.05.021.

19. M. Bernaas, I. Westermann, R. Johnsen, and M. Iannuzzi, "Effect of Microstructure on the Corrosion Resistance of Duplex Stainless Steels: Materials Performance Maps," paper presented at Corrosion 2017, New Orleans, LA, March 26–30, 2017 (NACE International, 2017), 1–15, https://doi.org/10.5006/C2017-08923.

20. H. M. Ezuber, "Metallurgical and Environmental Factors Affecting the Pitting Behavior of UNS S 32205 Duplex Stainless Steel in Chloride Solutions," *Materials and Corrosion* 63 (2012): 111–118, https://doi.org/10.1002/maco.201005667.

21. N. Larché, D. Thierry, V. Debout, et al., "Crevice Corrosion of Duplex Stainless Steels in Natural and Chlorinated Seawater," *Revue de Métallurgie* 108 (2011): 451–463, https://doi.org/10.1051/metal/2011080.

22. M. Kahram, M. Asnavandi, P. Koshy, and C. C. Sorrell, "Corrosion Investigation of Duplex Stainless Steels in Chlorinated Solutions," *Steel Research International* 86 (2015): 1022–1027, https://doi.org/10.1002/srin.201400293.

23. Y. Martinez-Galvan, L. Dzib-Perez, M. Garcia-Renteria, O. Bilyy, V. Lopez-Morelos, and J. Gonzalez-Sanchez, "Effect of Temperature on Resistance to Pitting Corrosion in Duplex Stainless Steel 2205 Welds," *Materials Science* 58 (2023): 755–761, https://doi.org/10.1007/s11003-023-00726-x.

24. L. F. Garfias-Mesias and S. R. Taylor, "In-Situ Pitting of UNS S32550 Duplex Stainless Steel in Artificial Seawater Below and Above the Critical Pitting Temperature," paper presented at Corrosion 2016, Vancouver, BC, March 6–10, 2016 (NACE International, 2016), 4597–4605, https://doi.org/10.5006/C2016-07837.

25. S. D. Kahar, "Duplex Stainless Steels—An Overview," *International Journal of Engineering Research and Applications* 7, no. 4 (2017): 27–36, https://doi.org/10.9790/9622-0704042736.

26. M. Breda, L. Pezzato, M. Pizzo, and I. Calliari, "Effect of Cold Rolling on Pitting Resistance in Duplex Stainless Steels," *Metallurgia Italiana* 106 (2014): 15–19, https://www.fracturae.com/index.php/aim/article/view/1403.

27. W. Gong, L. Zhang, L. Zhang, Z. Jiang, and E. Wang, "Influence of Ce Addition on Microstructure and Corrosion Resistance of 2101 Duplex Stainless Steel," *Steel Research International* 92, no. 8 (2021): 2100003, https://doi.org/10.1002/srin.202100003.

28. L. Pezzato, M. Lago, K. Brunelli, M. Breda, E. Piva, and I. Calliari, "Effect of Secondary Phases Precipitation on Corrosion Resistance of Duplex Stainless Steels," *Materials Science Forum* 879 (2016): 1495–1500, https://doi.org/10.4028/www.scientific.net/MSF.879.1495.

29. K. Ohashi, R. K. Hitachi, J. F. D. Stott, and M. J. Schofield, "Marine Crevice Corrosion of Stainless Steel Alloys Under Biofilmed and Sterile Conditions," paper presented at Corrosion 2016, Vancouver, BC, March 6–10, 2016 (NACE International, 2016), 372–386, https://doi.org/10.5006/C2016-07109.

30. P. Srisungsitthisunti, S. Daopiset, and N. Kanjanaprayut, "Crevice Corrosion of Duplex Stainless Steels by Cyclic Potentiodynamic Polarization and Potentiostatic Techniques," *Key Engineering Materials* 728 (2017): 123–128, https://doi.org/10.4028/www.scientific.net/KEM.728.123.

31. J. Ming, X. Zhou, and J. Shi, "Feasibility of Using 2304 Duplex Stainless Steel in Seawater-Mixed Concrete Pore Solutions: A Preliminary Passivation Consideration," *Construction and Building Materials* 438 (2024): 137037, https://doi.org/10.1016/J.CONBUILDMAT.2024.137037.

32. C. Gennari, A. F. Miranda-Pérez, L. Pezzato, M. Pigato, I. Calliari, and B. R. Rodríguez-Vargas, "Lean Duplex Stainless Steels Welded by LBW Subjected to Corrosion Testing," *MRS Advances* 9 (2024): 1887–1890, https://doi.org/10.1557/s43580-024-00981-3.

33. H. Y. Chang, H. B. Park, Y. S. Kim, S. K. Ahn, K. T. Kim, and Y. Y. Jang, "Compatibility Evaluation for Application of Lean Duplex Stainless Steels to Seawater Systems in Nuclear Power Plants," *Materials Science Forum* 654–656 (2010): 382–385, https://doi.org/10.4028/www.scientific.net/MSF.654-656.382.

34. "ASTM G150: Standard Test Method for Electrochemical Critical Pitting Temperature Testing of Stainless Steels," ASTM, 1999, https://www.astm.org/g0150-18.html.

35. "EN 10088-1: European Standard for Stainless Steels—Part 1: List of Stainless Steels, Brussels," SIST, 2023, https://cdn.standards.iteh.ai/samples/72863/d49a209463e043a1a6d10623552bde65/SIST-EN-10088-1-2024.pdf?utm_source=chatgpt.com.

36. D. M. Escriba, E. Materna-Morris, R. L. Plaut, and A. F. Padilha, "Chi-Phase Precipitation in a Duplex Stainless Steel," *Materials Characterization* 60 (2009): 1214–1219, https://doi.org/10.1016/j.matchar.2009.04.013.

37. "ISO 17781: Petroleum, Petrochemical and Natural Gas Industries—Test Methods for Quality Control of Microstructure of Ferritic/Austenitic (Duplex) Stainless Steels," 2017, https://www.iso.org/standard/60525.html.

38. "ASTM E1245: Standard Practice for Determining the Inclusion or Second-Phase Constituent Content of Metals by Automatic Image Analysis," ASTM, 2016, https://doi.org/10.1520/E1245-03R16.

39. "ASTM E562: Standard Test Method for Determining Volume Fraction by Systematic Manual Point Count," ASTM, 2020, https://doi.org/10.1520/E0562-19E01.

40. N. Sridhar, J. Kolts, and L. H. Flasche, "A Duplex Stainless Steel for Chloride Environments," *Journal of Metals* 37 (1985): 31–35, https://doi.org/10.1007/BF03258660.

41. "ISO 18070: Corrosion of Metals and Alloys-Crevice Corrosion Formers With Disc Springs for Flat Specimens or Tubes Made From Stainless Steel," ISO, 2015, https://www.iso.org/standard/61290.html.

42. "ASTM G4: Standard Guide for Conducting Corrosion Coupon Tests in Field Applications," ASTM, 1995, https://www.astm.org/g0004-01r14.html.

43. R. Francis and G. Byrne, "Corrosion Performance of 25% Cr Superduplex Stainless Steel for Different Seawater Applications," *Stainless Steel World* 16, no. 6 (2011): 53–58.

44. N. Larché, D. Thierry, P. Boillot, et al., "Crevice Corrosion Performance of High Grade Stainless Steels and Ni-Based Alloys in Natural and Treated Seawater," in Corrosion 2016, Vancouver, BC, March 6–10, 2016 (NACE International, 2016), https://doi.org/10.5006/C2016-07196.

45. N. Larché, C. Leballeur, E. Diler, and D. Thierry, "Crevice Corrosion of High-Grade Stainless Steels in Seawater: A Comparison Between Temperate and Tropical Locations," *Corrosion* 79 (2023): 1106–1117, https://doi.org/10.5006/4370.

46. ASTM International. *ASTM A967: Standard Specification for Chemical Passivation Treatments for Stainless Steel Parts* (ASTM International, 2005), https://doi.org/10.1520/A0967-05E01.

47. "Service d'Observation en Milieu Littoral (SOMLIT) Webpage," SOMLIT, 2024, https://www.somlit.fr/brest/.

48. N. Larché, B. Emo, A. Allion, E. Johansson, and D. Thierry, "Localized Corrosion of (Lean) Duplex Stainless Steels in Immersion Units of Urban Wastewater Treatment Plants," *Materials and Corrosion* 72 (2021): 1338–1349, https://doi.org/10.1002/maco.202112298.

49. D. Nakhaie, M. Zakeri, M. Naghizadeh, A. M. Clifford, and E. Asselin, "Statistical Distribution of Critical Pitting Temperature of Stainless Steels," *Journal of the Electrochemical Society* 170 (2023): 061504, https://doi.org/10.1149/1945-7111/acdcbe.

50. A. Delblanc, A. Iversen, and K. Lund, "Comparison of Critical Pitting Temperatures of Stainless Steels in Different Salt Solutions," paper presented at CORROSION 2018, Phoenix, Arizona, USA, April 2018 (NACE International, 2018), https://doi.org/10.5006/C2018-10846.

51. H.-Y. Chang, Y.-S. Park, and W.-S. Hwang, "A Study on the Modeling of Parameters Affecting the IR Drop Mechanism in the Initiation Stage of Crevice Corrosion," *Metals and Materials* 6 (2000): 505–511, https://doi.org/10.1007/BF03028091.

52. G. F. Kennell, R. W. Evitts, and K. L. Heppner, "A Critical Crevice Solution and IR Drop Crevice Corrosion Model," *Corrosion Science* 50 (2008): 1716–1725, https://doi.org/10.1016/j.corsci.2008.02.020.

53. B. Luo, Q. Hu, J. Liu, and F. Huang, "Effect of Crevice Gap on Crevice Corrosion Initiation and Development of 2205 Duplex Stainless Steel in NaCl Solution," *Journal of Materials Research and Technology* 21 (2022): 2584–2597, https://doi.org/10.1016/J.JMRT.2022.10.059.

54. N. Corlett, L. E. Eiselstein, and N. Budiansky, "Crevice Corrosion," in *Shreir's Corrosion*, eds. B. Cottis, M. Graham, R. Lindsay, S. Lyon, T. Richardson, D. Scantlebury, and H. Stott (Elsevier Science, 2010), 753–771, https://doi.org/10.1016/B978-044452787-5.00029-9.

55. R. W. Revie and H. H. Uhlig, *Corrosion and Corrosion Control: An Introduction to Corrosion Science and Engineering*, 4th ed. (John Wiley & Sons, 2008), https://doi.org/10.1002/9780470277270.

56. B. N. Popov, "Pitting and Crevice Corrosion," in *Corrosion Engineering* (Elsevier, 2015), 289–325, https://doi.org/10.1016/B978-0-444-62722-3.00007-0.

57. E. Bardal, J. M. Drugli, and P. O. Gartland, "The Behaviour of Corrosion-Resistant Steels in Seawater: A Review," *Corrosion Science* 35 (1993): 257–267, https://doi.org/10.1016/0010-938X(93)90157-C.

58. C. Marconnet, Y. Wouters, F. Miserque, et al., "Chemical Composition and Electronic Structure of the Passive Layer Formed on Stainless Steels in a Glucose-Oxidase Solution," *Electrochimica Acta* 54 (2008): 123–132, https://doi.org/10.1016/J.ELECTACTA.2008.02.070.

59. J. Landoulsi, K. E. Kirat, C. Richard, D. Féron, and S. Pulvin, "Enzymatic Approach in Microbial-Influenced Corrosion: A Review Based on Stainless Steels in Natural Waters," *Environmental Science & Technology* 42 (2008): 2233–2242, https://doi.org/10.1021/es071830g.

60. N. Le Bozec, C. Compère, M. L'Her, A. Laouenan, D. Costa, and P. Marcus, "Influence of Stainless Steel Surface Treatment on the Oxygen Reduction Reaction in Seawater," *Corrosion Science* 43 (2001): 765–786, https://doi.org/10.1016/S0010-938X(00)00113-X.

61. R. C. Newman, "2001 W.R. Whitney Award Lecture: Understanding the Corrosion of Stainless Steel," *Corrosion* 57 (2001): 1030–1041, https://doi.org/10.5006/1.3281676.

62. J. R. Galvele, "Tafel's Law in Pitting Corrosion and Crevice Corrosion Susceptibility," *Corrosion Science* 47 (2005): 3053–3067, https://doi.org/10.1016/J.CORSCI.2005.05.043.

63. S. Giriga, U. K. Mudali, V. R. Raju, and B. Raj, "Electrochemical Noise Technique for Corrosion Assessment—A Review," *Corrosion Reviews* 23 (2005): 107–170, https://doi.org/10.1515/CORRREV.2005.23.2-3.107.

64. M. S. B. Reddy, D. Ponnamma, K. K. Sadasivuni, et al., "Sensors in Advancing the Capabilities of Corrosion Detection: A Review," *Sensors and Actuators, A: Physical* 332 (2021): 113086, https://doi.org/10.1016/j.sna.2021.113086.

65. C. S. Brossia, K. Chiang, R. A. Cottis, et al., *Techniques for Corrosion Monitoring*, 2nd ed. (Woodhead Publishing, 2021), https://doi.org/10.1016/B978-0-08-103003-5.09992-6.

66. S. R. F. Batista and S. E. Kuri, "Aspects of Selective and Pitting Corrosion in Cast Duplex Stainless Steels," *Anti-Corrosion Methods and Materials* 51 (2004): 205–208, https://doi.org/10.1108/00035590410533156.

67. W. T. Tsai and J. R. Chen, "Galvanic Corrosion Between the Constituent Phases in Duplex Stainless Steel," *Corrosion Science* 49 (2007): 3659–3668, https://doi.org/10.1016/J.CORSCI.2007.03.035.

68. W.-T. Tsai, K.-M. Tsai, C. Lin, and Y. Fu, "Selective Corrosion in Duplex Stainless Steel," *Journal of Electrochemistry* 9 (2003): 170–176, https://doi.org/10.61558/2993-074X.1501.

69. A. Laitinen and H. Hänninen, "Chloride-Induced Stress Corrosion Cracking of Powder Metallurgy Duplex Stainless Steels," *Corrosion* 52 (1996): 295–306, https://doi.org/10.5006/1.3293641.

70. S. Lv, Z. Yang, B. Zhang, J. Chen, Y. Chen, and X. Li, "Corrosion and Passive Behaviour of Duplex Stainless Steel 2205 at Different Cooling Rates in a Simulated Marine-Environment Solution," *Journal of Iron and Steel Research International* 25 (2018): 943–953, https://doi.org/10.1007/s42243-018-0136-x.

71. H. Tan, Y. Jiang, B. Deng, T. Sun, J. Xu, and J. Li, "Effect of Annealing Temperature on the Pitting Corrosion Resistance of Super

Duplex Stainless Steel UNS S32750," *Materials Characterization* 60 (2009): 1049–1054, https://doi.org/10.1016/j.matchar.2009.04.009.

72. N. Larché, C. Leballeur, S. Le Manchet, and W. He, "Localized Corrosion of High-Grade Stainless Steels: Grade Selection in Chlorinated Seawater," *Corrosion* 79 (2023): 997–1005, https://doi.org/10.5006/4348.

73. F. Ruel, D. Tite, A. Gaugain, S. Saedlou, and K. Wolski, "On the Depassivation Mechanism of Lean Duplex Stainless Steels and the Influence of the Partitioning of the Alloying Elements," *Corrosion* 70 (2014): 636–642, https://doi.org/10.5006/1173.